University of Rhode Island and NOAA/NESDIS

BOASNRA Algorithm Theoretical Basis Document

Igor M. Belkin and collaborators

Version 6.0

April 14, 2014

TITLE: BOASNRA ALGORITHM THEORETICAL BASIS DOCUMENT VERSION 6.0

AUTHORS:

Igor M. Belkin (University of Rhode Island)

Other contributors:

Banghua Yan (NESDIS/OSPO)

Phillip Keegstra (NESDIS/STAR)

Menghua Wang (NESDIS/STAR)

Other NOAA CoastWatch Team Members (NESDIS/STAR)

DOCUMENT HISTORY
DOCUMENT REVISION LOG

The Document Revision Log identifies the series of revisions to this document since the baseline release. Please refer to the above page for version number information.

DOCUMENT TITLE: BOASNRA Algorithm Theoretical Basis Document			
DOCUMENT CHANGE HISTORY			
Revision No.	**Date**	**Revision Originator Project Group**	**Approval # and Date**
1.0	15 June 2012	Initial release by Igor Belkin	
2.0	4 September 2012	Second, updated release by Igor Belkin	
3.0	13 September 2012	Third, updated release by Igor Belkin	
4.0	12 April 2013	Fourth, updated release by Igor Belkin	
5.0	18 April 2013	Fifth, updated release by Igor Belkin	
6.0	14 April 2014	Sixth, updated by Banghua Yan	

LIST OF CHANGES

Significant alterations made to this document are annotated in the List of Changes table.

DOCUMENT TITLE: BOASNRA Algorithm Theoretical Basis Document					
LIST OF CHANGE-AFFECTED PAGES/SECTIONS/APPENDICES					
Version Number	**Date**	**Changed By**	**Page**	**Section**	**Description of Change(s)**

TABLE OF CONTENTS

Page

LIST OF TABLES AND FIGURES 6

1. INTRODUCTION 7

1.1. Product Overview 7
1.1.1. Product Description 7
1.1.2. Product Requirements 8

1.2. Satellite Instrument Description 8

2. ALGORITHM DESCRIPTION 9

2.1. Processing Outline 9

2.2. Algorithm Input 11

2.3. Theoretical Description 12
2.3.1. Physical Description 12
2.3.2. Mathematical Description 14

2.4. Algorithm Output 23

2.5. Performance Estimates 23

2.6. Practical Considerations 28
2.6.1. Numerical Computation Considerations 28
2.6.2. Programming and Procedural Considerations 28
2.6.3. Quality Assessment and Diagnostics 29
2.6.4. Exception Handling 29

2.7. Validation 29

3. ASSUMPTIONS AND LIMITATIONS 52

3.1. Performance Assumptions 52

3.2. Potential Improvements 52

4. REFERENCES 54

LIST OF TABLES AND FIGURES

Page

Page 6
Figure X – Figure Caption 6

Figure X – Figure Caption

Table X – Table Title

Note that these figure captions and table titles are generic placeholders. When actual figures and tables are inserted into the SMM, they should be numbered according to this convention:

The first figure for a given main section (e.g. Section 3) should be numbered Figure 3-1, etc.

The first table for a given main section (e.g. Section 2) should be numbered Table 2-1, etc.

1. INTRODUCTION

1.1. Product Overview

1.1.1. Product Description

The BOASNRA is a concatenation of two acronyms – BOA and SNRA. The BOA stands for the Belkin-O'Reilly Algorithm for front detection (Belkin and O'Reilly, 2009). The SNRA stands for the Stripe Noise Reduction Algorithm developed in 2011-2012 and not described yet in peer-reviewed literature. Both algorithms are documented in detail below. Since the SNRA takes advantage of the BOA, this document presents these two algorithms as a single entity, BOASNRA. This approach is most convenient to the user, both conceptually and operationally, because the BOASNRA is implemented as a single code. Throughout the rest of this document, we use "BOASNRA" and "the algorithm" interchangeably, unless explicitly stated otherwise.

The BOASNRA maps oceanic fronts from satellite imagery. Oceanic fronts are narrow zones of elevated gradients of properties such as temperature, salinity, nutrients, chlorophyll etc. (Belkin, 2002; Belkin, Cornillon, and Sherman, 2009). The BOASNRA was designed primarily to map fronts in chlorophyll (Chl) fields. The emphasis on Chl stems from the fact that Chl is most important to marine biota. Maps of Chl fronts can be directly used in marine fisheries, marine conservation, environment protection, and other applications and operations. The current experience with this algorithm has shown that the BOASNRA is quite universal. Of particular importance is the algorithm's successful application to sea surface temperature, SST (Hyde, O'Reilly, and Belkin, 2008; Belkin, Hyde, and O'Reilly, 2012). The algorithm has also been applied to sea surface height, SSH, from satellite altimetry, and to sea surface roughness, SSR, from the Synthetic Aperture Radar, SAR (Gary Borstad, private communication, 2012). Even though the BOASNRA has been shown to be quite universal, we only refer to Chl throughout this document.

The BOASNRA uses MODIS Aqua Level 2 fields (images) of Chl as input. Every elementary application of the algorithm involves a single image of Chl as input. The algorithm's output consists of several files. The algorithm generates fields of gradient magnitude and gradient direction that conform to the original field of Chl. The output values are calculated for each pixel of the original image. Details of input and output are described in respective sections below.

1.1.2. Product Requirements

The BOASNRA is developed to provide maps of oceanic fronts to diverse groups of end-users such as fisheries managers, professional and recreational fishermen, sailors, weather forecasters, naval oceanographers, research scientists, educators, marine environmental conservationists, and general public. Each group of users might have different interests and expectations yet their interests and expectations substantially overlap, which allowed product requirements to be formulated. The main requirement to frontal products generated to by the BOASNRA is their visualization as geographical maps that can be easily comprehended and navigated by an average end-user. Therefore during the development of BOASNRA a heavy emphasis was made on frontal mapping. By far the most important parameter of oceanic fronts is their ***location*** in a geographical reference frame. The second most important parameter is the ***frontal strength*** equated with frontal gradient magnitude. The next most important parameter is ***frontal orientation*** equated with frontal gradient direction. Consequently, the product requirements stipulate generation of two frontal maps per each satellite image: (1) map of gradient magnitude, GM; (2) map of gradient direction, GD. Most users require frontal maps to be highly detailed and not generalized or smoothed, so they expect frontal products to retain the original ***spatial resolution*** of satellite imagery. Therefore the frontal maps generated by the BOASNRA are pixel-based, with the pixel size equal to the spatial resolution of satellite imagery. Since the algorithm is developed for MODIS Aqua, this requirement means that frontal maps should have spatial resolution of 1 km. The ***image format*** of frontal maps must be fully portable across the whole spectrum of computers; JPEG and PNG, among other formats, provide such portability, while Web (online) publication of such maps provides the most convenient, fast, and cost-effective way of product dissemination. The next parameter of importance is ***latency*** as a measure of time delay between satellite data acquisition and generation of frontal products for end-users. Here expectations and requirements of different groups of users vary widely, from hours in mission-critical applications such as naval oceanography, search-and-rescue, and yacht-racing to a few days in ship route optimization, deep-sea fishing, and weather forecasting to months in fisheries management and years in marine environmental conservation and education. Fortunately, the available data processing system is capable of meeting all but the most stringent requirements of diverse customers by providing frontal maps within a few days of satellite data acquisition.

1.2. Satellite Instrument Description

The MODIS (Moderate Resolution Imaging Spectroradiometer) instrument is flown aboard the Aqua (EOS PM-1) satellite (http://modis.gsfc.nasa.gov/about/) launched on May 4, 2002 onto a low-Earth, Sun-synchronous orbit, with the following elements: semimajor axis, 7077.75 km; eccentricity, 0.001203; inclination, 98.14°; apoapsis, 708 km (440 mi); periapsis, 691 km (429 mi); orbital period, 98.4 minutes; orbits per day, 14.5625.

The MODIS Aqua provides high radiometric sensitivity (12 bit) in 36 spectral bands (from 0.4 µm to 14.4 µm), of which bands 8-16 are relevant to ocean color (see MODIS Aqua Technical Specifications below). A ±55-degree scanning pattern at the EOS orbit with a 708-km apoapsis achieves a 2,330-km swath and, combined with a near-polar, slightly retrograde orbit (inclination, 98.14°) provides global coverage every 1 to 2 days. The ocean color-relevant bands 8-16 are imaged at a nominal resolution of 1 km at nadir.

The MODIS Aqua Technical Specifications relevant to ocean color and chlorophyll:
Orbit: apoapsis, 708 km; periapsis, 691 km; 1:30 p.m. ascending node, sun-synchronous, near-polar, circular
Scan Rate: 20.3 rpm, cross-track
Swath Dimensions: 2330 km (cross-track) by 10 km (along-track at nadir)
Spatial Resolution of bands 8-16: 1000 m
Bands (bandwidth in nm): 8 (405-420), 9(438-448), 10(483-493), 11(526-536), 12(546-556), 13(662-672), 14(673-683), 15(743-753), 16(862-877).

2. ALGORITHM DESCRIPTION

2.1. Processing Outline

The processing outline of the BOASNRA algorithm is shown in a flowchart (Figure 2.1-1) and described below. Detailed descriptions of all steps are provided in the next sections.

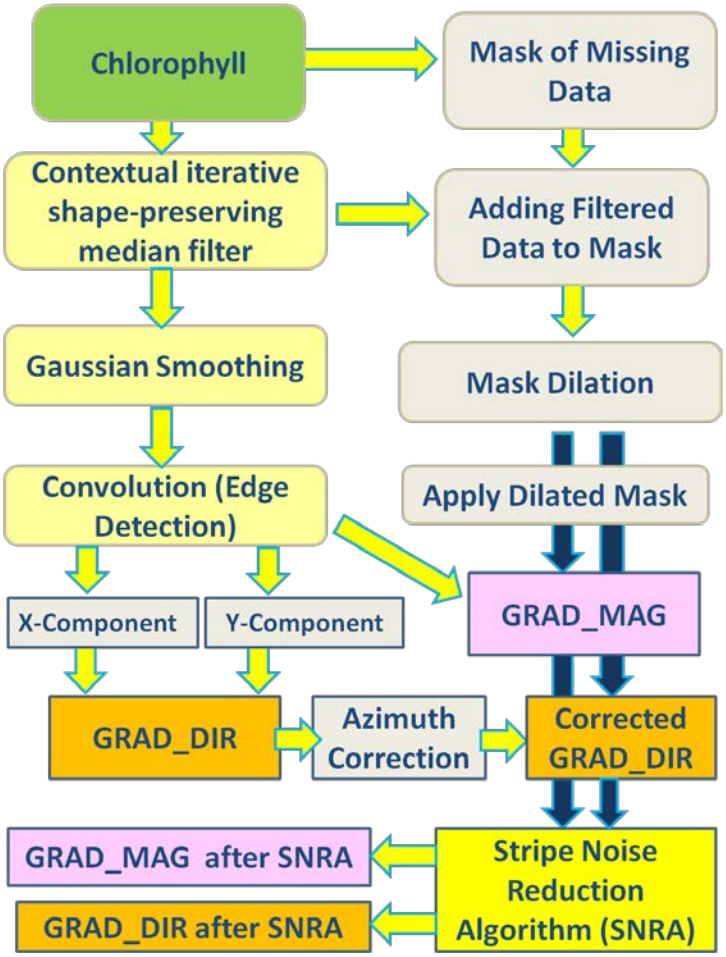

Fig. 2.1-1. Flowchart of the BOASNRA algorithm.

Chlorophyll arrays extracted from MODIS-Aqua Level 2 HDF files are used as input data into the algorithm. Cloud filled and suspect pixels are masked prior to processing. The first and most critical step is to apply a contextual adaptive shape-preserving median filter (CASPMF). The CASPMF performs two major tasks. It eliminates the so-called impulse noise, while at the same time preserves step-like and ramp-like fronts as well as peaks (blooms) and ridges (Chl enhancement line features typically associated with physical fronts). The next step is Gaussian smoothing, which suppresses high-frequency noise. The frontal edges are then detected by convolution, which outputs pixel-based gradients projected onto X- and Y-axis. From the X- and Y-components, gradient magnitude (GRAD_MAG) and gradient direction (GRAD_DIR) are calculated for each pixel. After applying azimuth correction to GRAD_DIR, both GRAD_MAG and GRAD_DIR are processed with the SNRA (Stripe Noise Reduction Algorithm), which reduces stripe noise often present in MODIS images. GRAD_MAG and GRAD_DIR are processed by SNRA

independently. After having been corrected by SNRA, both GRAD_MAG and GRAD_DIR are provided as the BOASNRA output.

2.2. Algorithm Input

The BOASNRA algorithm uses Level-2 Chl data from MODIS Aqua as input.

The Ocean Level-2 Data Products are described on the Ocean Color Web site maintained by the NASA Goddard Space Flight Center (http://oceancolor.gsfc.nasa.gov/DOCS/ocformats.html#3): The MODIS Level-2 product is generated from a corresponding Level-1B product. The chlorophyll-*a* concentration (denoted in this document simply as Chl) is derived from the Level-1B raw radiance counts by applying atmospheric corrections and bio-optical algorithms. The Level-2 product corresponds exactly in geographical coverage (scan-line and pixel extent) to that of its parent Level-1B product and is stored in one physical HDF file. Detailed information on the Level-2 format specifications can be found in the Ocean Level-2 Data Product document: http://oceancolor.gsfc.nasa.gov/DOCS/Ocean_Level-2_Data_Products.pdf "

The MODIS (Moderate Resolution Imaging Spectroradiometer) instrument is flown aboard the Aqua satellite (http://modis.gsfc.nasa.gov/about/). The Aqua MODIS provides high radiometric sensitivity (12 bit) in 36 spectral bands (from 0.4 µm to 14.4 µm), of which bands 8-16 are relevant to ocean color (see MODIS Aqua Technical Specifications below). A ±55-degree scanning pattern at the EOS orbit with an apoapsis of 705 km and a periapsis of 691 km achieves a 2,330-km swath and, combined with the near-polar orbit (inclination, 98.14°), provides global coverage every 1 to 2 days. The ocean color-relevant bands 8-16 are imaged at a nominal resolution of 1 km at nadir.

<u>The MODIS Aqua Technical Specifications relevant to ocean color and chlorophyll:</u>
Orbit: apoapsis, 705 km; periapsis, 691 km; 1:30 p.m. ascending node (local time of northward crossing of the equator); sun-synchronous; near-polar retrograde (inclination, 98.14°); circular.
Repeat cycle: 16 days.
Scan rate: 20.3 rpm, cross-track.
Swath dimensions: 2,330 km (cross-track) by 10 km (along-track at nadir*).
Spatial resolution (pixel size at nadir) of bands 8-16: 1000 m.
Bands (bandwidth in nm): 8 (405-420), 9(438-448), 10(483-493), 11(526-536), 12(546-556), 13(662-672), 14(673-683), 15(743-753), 16(862-877).
<u>*Note on the "bow tie" effect:</u> Unlike other scanning sensors (e.g., AVHRR), the along-track dimension of MODIS swath varies across track depending on viewing angle and increasing away from nadir, thereby causing the so-called "bow tie" effect, that is scan lines becoming wider and overlapping with one another at off-nadir angles.

2.3. Theoretical Description

2.3.1. Physical Description

Introduction
The BOASNRA consists of two algorithms, BOA and SNRA. BOA performs fronts detection, while SNRA performs stripe noise reduction. Formally, these two algorithms are independent and therefore are described in respective separate sections below. In practice, the BOASNRA works as a single algorithm implemented as a single code. The reason for merging both algorithm into a single algorithm and single code is obvious: By reducing stripe noise, the SNRA facilitates front perception and visual detection by the end user.

Front detection
The BOA was developed to detect fronts in satellite imagery of ocean color (proxy of chlorophyll concentration, Chl). This is the first-ever algorithm explicitly designed to detect Chl fronts. All previous algorithms (see Belkin and O'Reilly (2009) for a bibliography) were designed to detect SST fronts. Physically, Chl fronts are fundamentally different from SST fronts. Also, there are endemic features in Chl fields that are not encountered in SST fields, namely (1) Chl enhancement at physical (hydrographic) fronts and (2) point-wise Chl blooms. There are two reasons for Chl fronts to be fundamentally different from SST fronts. The first reason is that Chl is *concentration* (of a biologically active pigment), whereas SST is a scalar intensive physical property of sea water. When two adjacent water masses have different physical properties (for example, different temperature, salinity, and density), these water masses are separated by a physical front. In the great majority of cases, such fronts are associated with (a) geostrophic along-front currents and (b) surface convergence toward the front. These two processes are interconnected. The most important distinction between Chl and SST fronts is related to surface convergence. When two water masses with two different SSTs (T1>T2) converge, the frontal SST ranges from T1 to T2, that is the front temperature FT is intermediate between T1 and T2: T1>FT>T2. Owing to the surface convergence, the SST front is usually sharp and can be described by a step function or a ramp model (Belkin and O'Reilly, 2009).

The situation can be very different in case of Chl fronts. When two water masses with different concentrations of Chl (C1>C2) converge, the resulting cross-frontal pattern often features a sharp peak termed "chlorophyll enhancement" (Ryan et al., 1999a, 1999b). This phenomenon can be accounted by two mechanisms. The first mechanism involves mechanical concentration of algae containing chloroplasts. The most common algae, *Dinoflagellates* (among other things, they cause harmful algal blooms) range in size from about 5 to 2,000 micrometers or 0.0002 to 0.08 inch (*Britannica Online Encyclopedia*). As the concentration of algae peaks at a physical front (associated with surface convergence toward the front), so does the Chl concentration. The second process (or rather group of processes) involves biological dynamics that results in proliferation of algae at a physical

front, which causes Chl concentration to peak at the physical front. The second process may operate independently from surface convergence toward physical fronts.

Another phenomenon endemic to Chl is point-wise Chl blooms (PWCB). The radial structure of PWCBs is similar to the cross-frontal structure of Chl enhancement at physical fronts. Both structures can be described by a peak model (Belkin and O'Reilly, 2009). The PWCBs are ubiquitous in the ocean. The size of an individual PWCB can vary from O(100 m) to O(10 km). The existence of PWSBs is partly accountable for the observed patchiness of Chl distribution, which plays an important role in ecology of organisms that populate the surface layer. Another important aspect of PWCBs is their contribution to the total Chl content of the surface layer. Because of relatively small sizes of PWCBs, most of them probably go unreported. All previous algorithms for front detection tend to filter out the PWCBs as impulse noise.

The BOA is explicitly designed to retain such critically important features as Chl enhancement at physical fronts and Chl peaks (PWCBs). A key element of the BOA is a novel feature-preserving context-sensitive median filter. This filter suppresses impulse noise, with one-pixel spikes eliminated completely. This filter does not smooth out the most important features: It leaves intact (a) step-like and ramp-like Chl fronts, (b) Chl ridges ("roof edges") caused by Chl enhancement along line features (physical fronts), and (c) Chl peaks or PWCBs.

Stripe noise reduction

A significant percentage of satellite imagery provided by MODIS Aqua is corrupted by stripes that degrade image quality and hinder visual perception of fronts by end users. The stripes appear in Level 1 data. From there, they propagate to Level 2 products and eventually to Level 3 products. A great deal of effort was spent to reduce stripe noise. All previous attempts were focused on Level 1 data. The stripe noise reduction algorithm (SNRA) developed in this project works with Level 2 swath data. There are several advantages of working with stripes in Level 2 data over doing the same with Level 3 data. First and foremost, stripes in L2 are narrower and better defined than in L3, where same stripes are much wider and more diffuse. In L2, scans and stripes are always horizontal and straight, which greatly simplifies the design of SNRA. The typical width of stripes in L2 is 1-to-2 pixels, which means that such stripes can be eliminated by a 5-point orthogonal median filter running normally to these stripes in the vertical direction. Another key advantage of working with L2 data stems from the observed fact that stripes in L2 are equidistant. And yet another experimental fact that simplifies the design of SNRA for L2 data is an empirical relation observed between stripe width W and stripe spacing S, which is $W<0.5S$. This means that any orthogonal median filter with a window height H less than stripe spacing S but more than twice stripe width ($2W<H<S$) is optimal for stripe reduction because such a filter would never span more than a single stripe.

The equidistance of stripes in L2 obviates the need for stripe detector, which would otherwise be necessary (for example, in L3). The simplest stripe detector is based on autocorrelation function computed for all vertical slices normal to horizontal stripes. This approach is viable in case of non-equidistant stripes, allowing such stripes to be detected and indexed prior to running stripe suppressor to reduce striping noise. In our case, this approach was not required. In the future, this approach could be used in complicated situations when stripe spacing varies or stripes are not straight (curvilinear).

Another important physical quality of stripes is their brightness. Visual inspection of striping patterns in 3,500 Chl images obtained by MODIS Aqua over a two-month period from April 1 to May 31, 2012, has shown that the stripe brightness is not constant along each individual stripe. In those cases when stripe brightness is approximately constant along each stripe, the stripe brightness may change from one stripe to another. Moreover, relative brightness of stripes (relative to adjacent scans/rows) may also change from one stripe to another. It may also change, albeit rarely, along the same stripe, so a bright stripe becomes a dark stripe within the same scan/row. The above physical properties prevent usage of simple thresholding based on maximum brightness (or minimum brightness in case of dark stripes). These properties likewise prevent usage of advanced thresholding based on relative brightness. A case can be made for adaptive contextual thresholding based on dynamic relative stripe brightness. Such an algorithm, however, is bound to be quite complicated and not necessarily robust. Fortunately, the above physical properties of stripes in L2 do not present significant obstacles to orthogonal median filters applied normally to horizontal stripes.

2.3.2. Mathematical Description

Introduction

The advent of remote sensing from satellites has enabled global monitoring of oceanic fronts from space. The first property used for this purpose was sea surface temperature, SST. In a seminal worldwide survey of oceanic fronts, Legeckis (1978) demonstrated a variety of SST fronts formed by vastly different physical processes — water mass convergences, river outflows, tidal mixing, coastal and open ocean upwelling etc. These processes create sharp horizontal gradients of SST identified with thermal fronts.
Such gradient zones or “edges” can be detected in SST imagery by objective methods. Two approaches became widely accepted: the gradient method thanks mainly to its simplicity (e.g. Kazmin and Rienecker,1996; Moore et al.,1997,1999; Kostianoy et al., 2004; Breaker et al., 2005); and the histogram method (Cayula and Cornillon, 1992, 1995, 1996), owing to its robustness and ample worldwide validation (Kahru et al., 1995; Belkin et al., 1998; Ullman and Cornillon, 1999; Ullman and Cornillon, 2000; Hickox et al., 2000; Belkin et al., 2001; Ullman and Cornillon, 2001; Mavor and Bisagni, 2001; Belkin et al., 2003; Belkin and Cornillon, 2003, 2004, 2005; Nieto and Demarcq, 2006; Miller, 2009; Belkin, Cornillon, and Sherman, 2009). Other methods have been tried as well, notably the Canny (1986) edge detector (e.g. Castelao et al., 2006; Nieto and Demarcq, 2006), the Holyer and

Peckinpaugh (1989) cluster-shadow method (e.g. Cayula et al., 1991), and the Vazquez et al. (1999) entropic approach (e.g. Shimada et al., 2005).

Thermal fronts enjoyed much-deserved attention partly because of widely available high-quality global imagery from NOAA satellites that extends back to mid-1980s. Oceanic parameters other than SST were not widely available until 1997 when SeaWiFS ocean color imagery became available, ushering in the era of global monitoring of estimated chlorophyll-a (Chl) concentration from space. The sheer and ever increasing volume of color imagery called for objective methods of its analysis; in particular, automatic detection of chlorophyll fronts has been widely recognized as a high-priority task (Chan, 1999; Bontempi and Yoder, 2004; Stegmann and Ullman, 2004; Miller, 2004; Nieto and Demarcq, 2006; Miller, 2009). And yet progress in this direction was limited, especially when compared with automatic detection of SST fronts. The most fundamental reason for this lies in the inherent complexity of Chl field versus SST, with Chl featuring spatial patterns that do not exist in SST, namely Chl blooms and Chl enhancement at thermohaline fronts. This fundamental difference between Chl and SST fields is illustrated by two respective conceptual models of a generic front separating shelf and oceanic waters usually called the shelf–slope front, SSF, or shelf break front (Fig. 2.3-1). A typical SST or Chl front can be modeled as a step function or *ramp* since the front is a sharp boundary between two relatively uniform water masses with different temperatures or Chl concentration (Fig. 2.3-1, top left). This simple structure can be seen in a Chl image of the SSF off the U.S. Northeast (Fig. 2.3-1, top right). However, the same front during a different season or year may appear quite differently in Chl field. The most peculiar cross-frontal structure characteristic of Chl field features elevated Chl peaking on – or close to – a respective TS-front. This phenomenon is called *chlorophyll enhancement* (at a hydrographic (physical) front); its transverse structure can be modeled as a *peak* (Fig. 2.3-1, bottom left). The Chl image of the SSF off the U.S. Northeast (Fig. 2.3-1, bottom right) shows a large-scale Chl enhancement extending over 1000 km along the SSF; similar patterns have been repeatedly observed and extensively studied in this area (Marra et al., 1990; Ryan et al., 1999a, b; Stegmann and Ullman, 2004). The exact form of the peak model may vary in the above concept that simply illustrates profound differences often observed between SST and Chl patterns in frontal zones.

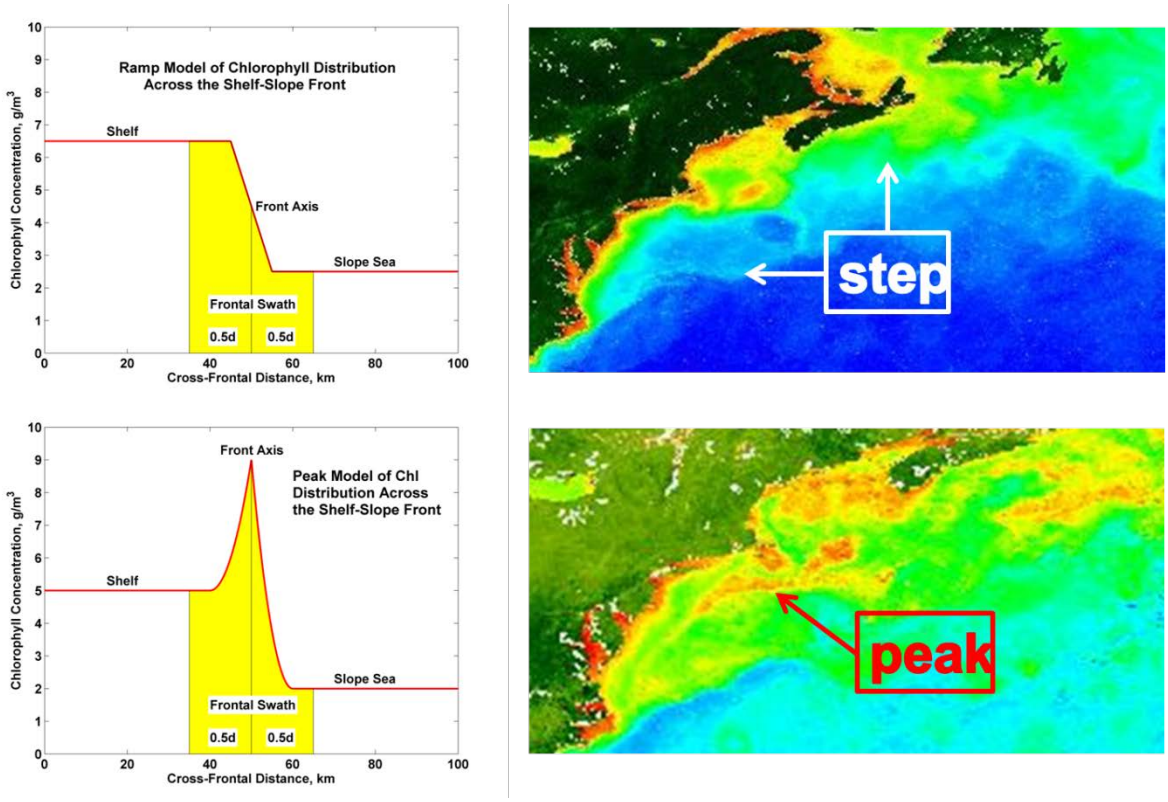

Fig. 2.3-1. Two types of Chl fronts. Modified after Belkin and O'Reilly (2009).

Another important aspect of the Chl field is *patchiness* on a variety of scales, evident from ocean color imagery and *in situ* data. Spatial structure of Chl field is a product of interplay of physical, chemical, and biological processes, and therefore is inherently more complex than the structure of physical fields such as temperature and salinity. Patchiness is a hallmark of Chl field. It may be formed by physical dynamics, e.g. by the underlying patchiness of the TS-field, and it may also be formed by biological dynamics; it may also result from physical–biological interactions and feedbacks. The observed richness of spatial patterns and features in the Chl field defies a simplistic approach to front detection based on a single model of cross-frontal transverse structure, be it a step, ramp, peak, or patch. However, there is a common feature associated with the various patterns, which is the *local maximum gradient*. This brings us back to the gradient method and its basic problem: noise. Since every differentiation (gradient computation) results in noise amplification, the noise should be dealt with before front detection/feature extraction. By developing and validating a new front detection algorithm, Belkin and O'Reilly (2009) demonstrated that effective noise suppression combined with feature preservation allows spatial gradients to be computed and mapped in a way that brings out diverse frontal patterns in the Chl field as well as SST fronts.

Front detection algorithm

The BOASNRA algorithm is designed specifically for detecting main features in Chl imagery (Belkin and O'Reilly, 2009). It is based on the following premise derived from (a) our experience in satellite frontal oceanography and (b) latest developments in digital image processing and pattern recognition: Fronts and other features of interest such as Chl peaks (blooms) and Chl enhancement at physical (hydrographic) fronts (Ryan et al., 1999a, b) can be revealed in satellite images by a contextual adaptive filter that removes noise but preserves these features. This filter thus is called *feature-preserving* or *shape-preserving* because it preserves the shape of well-defined sharp extrema. This is the first and main step performed by the algorithm. The second step is traditional in edge detection: since the features of interest are characterized by enhanced gradients, an edge detector, e.g. Sobel operator, brings out these features in images that have been processed with the contextual adaptive feature-preserving filter.

The *median filter* (MF) is a highly efficient technique of digital filtering that removes isolated noise while preserving edges in data. When applied to a one-dimensional (1D) array, MF replaces the central value of a sliding window of an odd size by the median of sorted (ranked) data from this window. When applied to an image, MF first converts each window matrix to a 1D array, then proceeds as above. MF is used as a pre-processing step of other front detection algorithms (e.g. Cayula and Cornillon, 1992, 1995). Thanks to its edge-preserving property, we have chosen MF for the first step of our front detection algorithm. At the same time, it was necessary to eliminate another – undesired – property that standard MF shares with all other digital filters; this property can be called *extremum alteration*. Indeed, standard MF always alters peaks and ridges by clipping them. In other words, standard MF degrades isolated sharp extrema and roof edges by making them blunt. This property is especially detrimental to, and therefore not acceptable in, any algorithm for feature extraction from Chl field since sharp isolated extrema (peaks) correspond to local Chl blooms, while ridges (roof edges) correspond to Chl enhancement at fronts — and both features are common in Chl fields.

To avoid extremum alteration, the digital filter must be able to recognize sharp extrema (peaks) and ridges (roof edges) – and leave them intact. In other words, the filter has to be *context-sensitive* and *selective* (*adaptive*). The central novel idea of our median filter is that it considers a small window within a larger context; therefore this method can be called *contextual median filter*. In oceanography, the first contextual median filter was developed for automatic classification of vertical profiles; it was validated on large climatological data sets from the North Pacific (Belkin, 1986, 1991). Since vertical profiles are 1D arrays, all possible 1D configurations of sharp extrema were explicitly described by a set of inequalities and hard-coded into a selective MF. This approach has been extended into 2D and applied to satellite imagery by Belkin and O'Reilly (2009). Specifically, satellite data (Chl values) from a sliding 3×3-pixel window are considered within the context of a larger 5×5-pixel window. The main problem in 2D is that there are too many possible

configurations of 2D sharp extrema and roof edges to be explicitly described by a set of inequalities; this would be impractical. Instead, the contextual MF performs its task in three steps:

(1) It makes all possible omni-directional 1D slices across the center of a sliding 5×5-pixel 2D window;
(2) It analyzes these slices;
(3) It makes a decision whether to filter the window's central pixel or leave it intact.

The above description of the algorithm is elaborated below as a pseudo-code:

Contextual median filter (MF3in5) pseudo-code

1. Check for peaks and troughs within 1D 5-point slices through a sliding 5×5 window. The window slides east–west (E–W), north–south (N–S) across the image:

```
for I=3:NROWS-2
        for J=3:NCOLS-2
                Make the WE slice across the window center A(I,J);
                Make the NS slice across the window center A(I,J);
                Make the NW–SE slice across the window center A(I,J);
                Make the NE–SW slice across the window center A(I,J);
                If the window center A(I,J) is a 5-point minimum or maximum along all four 5-
                point 1D slices, flag it as Peak-5
        end
end
```

2. Check for peaks and troughs within 1D 3-point slices through sliding 3×3 window. The window slides west–east, north–south across the image:

```
for I=3:NROWS-2
        for J=3:NCOLS-2
                If the window center A(I,J) is a 3-point maximum or minimum in 2D, mark it as
                Peak-3
        end
end
```

3. Apply the selective 2D 3×3 median filter within sliding 3×3 window. If the window center is a significant 5-point extremum (Peak-5), leave it intact (do not blunt it with median filter), otherwise if the window center is a spike (Peak-3) use the 2D 3×3 median filter:

```
for I=3:NROWS-2
        for J=3:NCOLS-2
                if (Center is Peak-5) skip the 3×3 Median Filter
                elseif (Center is Peak-3)
```

```
                    apply the 3×3 Median Filter
            end
        end
end
================== end of pseudo-code ============================
```

The above description and pseudo-code explain how contextual MF works during a single pass over a satellite image. In many applications, median filters are only applied once, as a single pass, since computational cost of *iterative* MF is often believed to be prohibitive. In reality, however, the iterative MF is quite efficient and computationally inexpensive owing to the following properties (Gallagher and Wise, 1981):

(1) Iterative MF in 1D always converges: After a number of iterations, the next iteration does not alter the signal;
(2) Iterative MF converges to the so-called *root signal*, which is *locally monotonous* that is the root signal consists of monotonous segments (ramps) and plateaus.

Iterative MF converges fast: The number of iterations until convergence, NITER, does not exceed (N−2)/2, where N is the number of data points in the 1D array to be filtered. Since NITER is a linear function of N, iterative MF converges much faster than most digital filters, whose convergence rate depends nonlinearly on the number of data points; typically, NITER~N^2. In our experiments with model (synthetic) images described below, MF converged after a few iterations. In test experiments with real satellite images the rate of convergence was slower. This issue is addressed below in the section about testing the algorithm.

There are two varieties of median filters: *recursive* and *non-recursive* (standard). The recursive filter uses part of its output on the previous step as part of its input during the next step. The standard MF is non-recursive. The MF used in the BOASNRA is non-recursive (standard). Even though recursive MF has certain advantages over non-recursive MF (e.g., Qiu, 1996), practical implementation of recursive MF is more complex than that of standard MF (Stork, 2003). Therefore we have chosen the standard approach. Our previous experiments with MF have shown that the output (root signal) is not overly sensitive to the choice between recursive vs. non-recursive MF.

Noise removal and smoothing

Since we are interested in preserving even relatively small-scale features, just a few pixels across, we do not use any smoothers, e.g. Gaussian, often used in applications elsewhere. In those applications, the signal (object) has a substantially larger scale, which is typically at least an order of magnitude larger than the noise; therefore a smoothing operator might improve the object's visibility in the image. In our case, the signal-to-noise scale ratio can be as small as 3, e.g. 3-pixel Chl peaks versus 1-pixel spikes. Therefore, in our situation,

any smoothing could be detrimental to gradient computation and climatology of relatively small but biologically important features in Chl field.

Gradient computation

The gradient vector is computed by the Sobel operator consisting of two 3×3 convolution masks or kernels: GX=[−1 0 +1;−2 0 +2;−1 0 +1]; and GY=[+1 +2 +1; 0 0 0; −1 −2 −1]; GY is simply GX rotated 90 degrees counter-clockwise. These kernels are used to calculate two images, Gx and Gy respectively, containing approximations for derivates in X and Y directions. If A is the original image, then Gx=GX*A and Gy=GY*A, where * is the convolution sign. At each point of the image, gradient magnitude and direction are computed as GM=sqrt(Gx^2+Gy^2) and GD=arctan(Gy/Gx) respectively. The Sobel operator is known as a simple and effective way of enhancing visibility of edges in digital images and iswidely used in a variety of applications, partly owing to its ultimate simplicity.

Gradient mapping: log-transformation of Chl data

Chlorophyll distribution on the global scale is approximately lognormal (Campbell, 1995). Therefore Chl data are usually log-normally transformed before any processing, mapping and statistical evaluation (e.g. Gregg and Conkright, 2001; Gregg and Casey, 2004). We have computed global Chl distribution from SeaWiFS, 1997–2007 (not shown) to confirm earlier findings based on spatially limited or irregular data (e.g. Campbell, 1995). We have also found a similar lognormal distribution in our test area (western North Atlantic) which encompasses shelf, slope and Sargasso Sea water and the three-orders-of magnitude range in surface Chl. Therefore we have *log-normally transformed* original Chl data and calculated Chl gradient from the log-normally transformed data. Our *logarithmic gradient* of Chl at every pixel is the difference between natural logarithms of Chl at adjacent pixels that is the natural *logarithm of the ratio* of adjacent Chl values.

Stripe Noise Reduction Algorithm

The MODIS images are known to be corrupted by stripes. Several groups in various countries developed different approaches to stripe noise reduction in Level-1 imagery (Rakwatin et al., 2007, 2009; Tsai and Chen, 2008; Di Bisceglie et al., 2009; Shen and Zhang, 2009; Bouali and Ladjal, 2011; Shen et al., 2011; Gladkova et al., 2012; see also the recent destriping software for Level-1 imagery developed at the University of Wisconsin, available at http://cimss.ssec.wisc.edu/imapp/destripe.shtml). Most developments in this field have taken advantage of hardware-related specifics of Level-1 data, down to minute details of satellite detectors and their performance. At the same time, some ideas put forth by these researchers could be applied to Level-2 and Level-3 imagery. Yet no attempts have been made to develop an algorithm dealing with stripes in Level-2 or Level-3 imagery. A careful examination of stripes in Level-3 imagery has shown that these stripes are often broad and diffuse (poorly defined) compared with stripes in Level-1 imagery and Level-2 imagery. Also, owing to image georegistration procedure, stripes in Level-3 imagery may have arbitrary orientation and may be curvilinear. Dealing

with curvilinear stripes of arbitrary orientation is a formidable problem of pattern recognition and image processing. We were unaware on any successful attempt at solving this problem. Therefore we focused our efforts on developing an approach suitable for Level-2 imagery since dealing with stripes in Level-2 imagery offers critical advantages vs. Level-3 imagery.

We developed a relatively simple stripe noise reduction algorithm (SNRA hereafter; see the SNRA flowchart in Fig. 2.3-2) for Level-2 imagery.

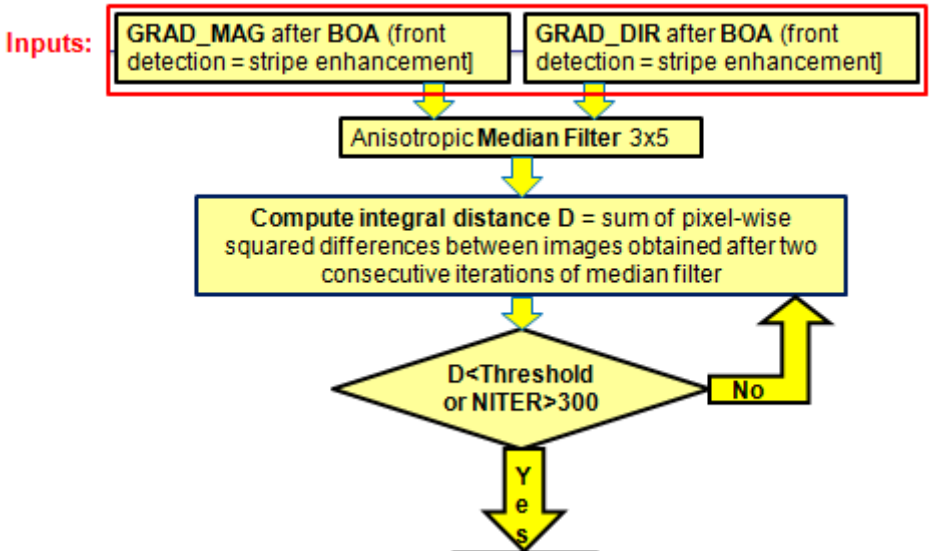

Fig. 2.3-2. Flowchart of the SNRA algorithm.

The SNRA takes advantage of a few properties of stripes in Level-2 imagery, namely:

(1) Stripes have the same orientation, being always horizontal;
(2) Stripes are always straight;
(3) Stripes are relatively narrow, typically two pixels wide;
(4) Stripe width is fairly constant along the same stripe;
(5) Stripe spacing is often constant within the same image.

At the same time, the MODIS stripe patterns have two properties that complicate the situation, namely:

(1) Stripe spacing may vary within the same image;
(2) Stripe width may vary from one stripe to another.

The SNRA also takes advantage of the BOA front detection algorithm. It was noticed that the BOA works as stripe enhancer since stripes are treated by the contextual adaptive shape-preserving median filter (CASPMF) as the so-called *roof edges* or ridges. These features are considered as just another type of fronts in addition to the common stepwise (or ramp-like) fronts. In other words, the BOA brings out stripes in MODIS data, thereby facilitating stripe noise reduction. Therefore the SNRA runs right after the BOA. Both

algorithms are implemented together as a single computer code and for all practical means and purposes can be considered as a single algorithm, the BOASNRA.

Since stripes in Level-2 imagery are straight and horizontal, it is natural to use one-dimensional median filter running normally to the stripes that is vertically. Since stripes are narrow (typically just two pixels wide), they can be reduced (if not completely eliminated) by iterative median filter with the window height WH, which satisfies the following condition: WH > SW*2, where SW is stripe width. At the same time, WH should be significantly less than stripe spacing SS, otherwise the window would span two stripes at once, which is not acceptable. Therefore, WH should meet the following condition: WH < SS – SW. As a result, WH should meet the double restriction: SW*2 < WH < SS-SW. Remember also that the median filter window height should be an odd number. From our extensive experience with MODIS images and stripe patterns, typical values of the above parameters are: SW=2 and SS=8 to 10. These values result in the following double condition for WH: 4 < WH < 6 to 8. Thus WH should be either 5 or 7. We have chosen the least value out of these two, 5. The reason for choosing the minimum acceptable value of the window height is dictated by our goal of making the algorithm (SNRA) minimally invasive. In other words, we made sure that our median filter is the least smoothing one since low-frequency smoothing is considered highly detrimental to the output product quality. In the same vein, we selected the minimum value for the 2D median filter's width, which is 3. As a result, we settled on an anisotropic 2D median filter with the window width of 3 and window height of 5.

The 2D 3x5 median filter slides over the image horizontally and vertically. After each pass (iteration), a distance DIST2 between the output image and input image is computed as an integrated pixel-based squared difference between respective matrices. This parameter (DIST2) is a quantitative measure of improvement thanks to the median filter. The process iterates until convergence or until a certain threshold is reached or until a certain number of iterations. In one dimension, convergence of median filter is guaranteed (Gallagher and Wise, 1981). In two dimensions, there is no theoretical guarantee of convergence. Pathological cases can be constructed where median filter oscillates indefinitely between two states (images). Practically, two-dimensional filter always converges, although the convergence rate might be rather slow depending on circumstances. To prevent a drawn-out iteration process with no substantial improvement in the output quality, we set the maximum number of iterations at 300. This is a fairly arbitrary value. In practice, even 10 to 20 iterations are enough to exhaust median filter. Any further improvement is not significant.

The SNRA is applied to gradient magnitude and gradient direction independently (see the BOASNRA flowchart in Fig. 2.1-1 and SNRA flowchart in Fig. 2.3-2). Certain improvements are envisioned for future SNRA developments, particularly regarding gradient direction. These future upgrades are outlined in section 3.2 ("Potential Improvements").

Cloud masking and cloud mask dilation
The cloud flagging is done as part of the generation of the Chl product. In the SeaDAS's l2gen function (NASA's ocean color processing software), L2_Flags (level 2 flags) is a standard output included in the Level-2 HDF file and one of the flags representing clouds. The mask dilation's purpose is to ensure cloud edges are masked in addition to the clouds. This step is based on the mathematical morphology approach by Haralick et al. (1987).

Azimuth correction
During this step, the gradient direction is corrected to true north. The azimuth correction is an optional step.

2.4. Algorithm Output

The BOASNRA output consists of two major products, which are fields of gradient magnitude (GRAD_MAG) and gradient direction (GRAD_DIR), accompanied by auxiliary products, which are Cartesian components of the gradient vector, namely X-component and Y-component.

2.5. Performance Estimates

Introduction
The BOASNRA performance has been estimated using a large test data set (TDS hereafter). The TDS consists of all available MODIS Aqua Ocean Color data over a 2-month period from April 1, 2012 through May 31, 2012. These data are archived at the NOAA's Comprehensive Large Array-data Stewardship System (CLASS, www.class.noaa.gov) maintained by the NODC. Total number of data files that comprise TDS is 3,499. All data are archived as HDF files. Total volume of TDS is 154 GB.
The TDS has been processed with the BOASNRA C++ code on a dedicated platform, Lenovo IdeaCentre K330-77472KU desktop, with the following specifications: Intel Pentium processor G630 with 2 processing cores, 1333MHz system bus, 3MB cache and 2.7GHz processor speed; 6GB DDR3 SDRAM; and 1TB Serial ATA 7200 rpm hard drive. The BOASNRA C++ code was run under Ubuntu, a Linux-type operating system.

The processing of 3,499 HDF data files has taken approximately 70 hours, or approximately 1 min. per data file. The most computer-intensive part of the algorithm is iterative two-dimensional median filter. There are several parameters of the median filter that determine performance of the entire algorithm. These parameters are width W and height H of the median filter, threshold TH used to stop iterations, and the maximum allowable number of iterations NITER. Parameters W and H are fixed: W=3 and H=5. Threshold TH is defined in relative terms. For example, TH can be defined for the mean absolute difference (or mean squared difference) between two consecutive iterations divided over variance of the image. Median filters are known to converge, and they are known to converge fast. For one-dimensional median filters, convergence to a locally-

monotonous root signal is guaranteed, with convergence rate established: Any series of N elements processed with median filter converges after no more than (N-2)/2 iterations (Gallagher and Wise, 1981). The (N-2/2) is the upper bound for converge rate. In practice, median filters converge many times faster than (N-2/2).

However, the BOASNRA uses two-dimensional median filters. For two-dimensional median filters, convergence is not theoretically guaranteed. In some extremely rare ("pathological") cases, two-dimensional median filter might oscillate indefinitely between two stable modes. To prevent this from happening, the algorithm has a circuit breaker that stops iterations after a certain number of iterations, NITER. Normally, the process stops when difference between two consecutive iterations becomes less than TH. Otherwise, the process stops after NITER iterations. Experiments with median filters have shown that the size of the filter ("window size") is not critically important for performance as long as this size is relatively small. In our case, the median filter operates with a sliding 3x5 window, which means that every step involves sorting a data set of 15 real numbers within this window. In fact, the algorithm implements a median finder function that does not require sorting of the window subset. This function, albeit not crucially important, provides some performance improvement compared with standard median finders that use complete sort of window subset, for example bubble sort function.

Numerical experiments with NTER were conducted by varying it widely. The total CPU time changed little with NITER ranging from 10 to 200. The threshold TH affects performance less than NITER. Overall, the algorithm is quite robust. Its performance changes little when two free parameters (TH and NITER) vary within realistic ranges.

Since the BOASNRA consists of two algorithms (BOA+SNRA) that perform different functions, the performance of these algorithms can be assessed separately. The BOA is a front detector, while the SNRA performs stripe noise reduction. However, in practice these two algorithms are merged into a single algorithm (BOASNRA) implemented as a single code. Moreover, whereas the BOA performance – in principle – can still be assessed separately by outputting BOA results prior to passing them to SNRA, the SNRA performance can only be assessed in a context of the entire BOASNRA since the SNRA operates using the BOA output as its input.

Qualitative assessment of performance with regard to front detection

The BOA performance was assessed quantitatively and qualitatively in a synthetic image generation (SIG) environment; it was shown that the BOA is robust and invariant to scale, rotation, and background (Belkin and O'Reilly, 2009). A large-scale validation and qualitative assessment effort was undertaken in 2007-2009, when the BOA was run over >6,000 images of Chl and SST obtained for the U.S. Northeast in 2002-2011. Climatology of Chl and SST fronts for the U.S. Northeast was compiled based on 10 years of MODIS Aqua data. The main reason for the parallel usage of Chl and SST frontal climatologies was

two-fold: (1) Chl fronts are excellent markers of SST fronts, especially in summer when many SST fronts all but disappear after being obliterated by spatially uniform surface warming; (2) Another, independent climatology of SST fronts was previously obtained using the Cayula-Cornillon algorithm (CCA) based on a completely different approach called histogram method (Belkin, Cornillon, and Sherman, 2009). The BOA-generated Chl frontal maps were compared with the collocated CCA-generated maps of SST fronts for the same months. The comparison was made in the following areas: South Atlantic Bight, Mid-Atlantic Bight, Nantucket Shoals, Georges Bank, Gulf of Maine, and Nova Scotian Shelf. The BOA- and CCA-generated maps compare quite favorably. All fronts identified by CCA have been identified by BOA. At the same time, the BOA-generated maps revealed many small-scale and meso-scale fronts that have not been previously reported. The most conspicuous examples are newly-identified fronts over the Nantucket Shoals and Georges Bank. These fronts persist year-round, which can be explained by topographic steering. Spatial gradients associated with these features are quite strong. The bathymetrically-induced stability combined with strong spatial gradients renders these fronts important to fisheries and navigation. Results of this investigation are reported in detail by Belkin, Hyde, and O'Reilly (2012).

Quantitative assessment of performance with regard to stripe noise reduction
The stripe-reduction performance of the BOASNRA was assessed by running it over the above-described Test Data Set (TDS) of 3,499 images of ocean color. The Stripe Noise Reduction Algorithm (SNRA) has been developed to reduce stripe noise in MODIS Aqua Chl-a Level 2 imagery. The SNRA takes advantage of certain features of L2 data:

(1) Each image consists of scans obtained normally to flight direction;
(2) Each scan is represented by one row in data file;
(3) Stripes are aligned in along-scan direction (no cross-scan stripes);
(4) Stripes are horizontal in data image (array);
(5) Stripes are straight (unlike stripes in L3 data, after georegistration);
(6) Stripes are equidistant (at least, the great majority of stripes).
(7) After BOA, stripes in GM and GD are narrow, typically 2 pixels across.

The SNRA is designed to be applied to gradient magnitude (GM) and gradient direction (GD) generated by the BOA front detection algorithm. By applying SNRA to BOA products, advantage is taken of the BOA thanks to the observed fact that stripes are better defined in GM and GD after front detection by BOA compared to the same stripes in original Chl-a images. Particularly and practically, "better defined" means that stripes are narrow. This has profound implications for SNRA because it means that such stripes can be reduced by median filters running normally to the stripes, with median filter window height MFWH larger than twice stripe width SW yet smaller than stripe spacing SS (= stripe-to-stripe distance). These conditions can be written as a double inequality: $2*SW < MFWH < SS$.

Performance of SNRA can be measured using vastly different metrics that have been developed for digital filters. Many of these metrics have been developed specifically for median filters, and in most cases their authors were mostly concerned with removal of impulse noise , which is an important problem in satellite image data processing (Al-Amri et al., 2010; Bovik, 1987; Celebi et al., 2007; Curran and Dungan, 1989; Juhola et al., 1991; Kober et al., 2003; Konnik, 2009; Kumar et al., 2007; Liu et al., 2006; Mao and Gan, 1993; Melange et al., 2011; Nichol and Vohora, 2004; Olsen, 1993; Russell and Sinha, 2001; Sahasrabudhe et al., 1999; Tai and Yang, 2008; Wang and Bovik, 2002; Williamson et al., 1993; Wilson et al., 1997; Wu and Tang, 2011; Yang et al., 2009; Yang and Lai, 1996; Zhou et al., 2002). Some metrics were developed for evaluating destriping algorithms designed for L1 imagery.

Of many available metrics, we have chosen two: mean absolutely estimate (MAE) and mean squared estimate (MSE). The below pseudo-code describes the modified BOASNRA and applies to a single run of the modified BOASNRA code. In other words, the pseudo-code describes the processing of a single data file.

Pseudo-code of the Modified BOASNRA (= BOASNRA-TEDMF)
TEDMF = TEsting and Documenting (performance of) Median Filter.
DATA = Read MODIS Aqua OC L2 data (one data file); Make IMAGE(DATA)
Run the BOA part of the BOASNRA code:
Comment: The BOA part generates GRAD_MAG (=GM) and GRAD_DIR (=GD) files.
Make IMAGE(GM) and IMAGE(GD)
Calculate Variance of Image (in both GM and GD):
Use function ***Stripe Noise Estimator*** (below) to calculate Mean Absolute Estimate (MAE) and Mean Squared Estimate (MSE) of ***variance of image***, using sliding windows:
[MAE3, MSE3] = SNE(image, 3); [MAE5, MSE5] = SNE(image, 5)
[MAE7, MSE7] = SNE(image, 7); [MAE9, MSE9] = SNE(image, 9)
Run the SNRA part of the BOASNRA:
Iterate MEDIAN FILTER until convergence (diff<threshold) or until 30 iterations.
Make IMAGE(GM) and IMAGE(GD).
Calculate Variance of Image (in both GM and GD):
[MAE3, MSE3] = SNE(image, 3); [MAE5, MSE5] = SNE(image, 5);
[MAE7, MSE7] = SNE(image, 7); [MAE9, MSE9] = SNE(image, 9);
Calculate number of iterations until convergence (=NITER).
Calculate number of pixels modified by SNRA (=NPixMod).
Calculate MAE and MSE of ***difference*** between the same images before and after SNRA:
MAE=SUM(ABS(A(i,j)-B(i,j)))/NValPix; % NValPix=number of valid pixels
MSE=SUM (A(i,j)-B(i,j))^2)/NValPix;
A is image before SNRA; B is the same image after SNRA.
Both MAE and MSE are calculated for images of GM and GD, before and after SNRA.
========== end of pseudo-code ==========

The next pseudo-code describes the ***Stripe Noise Estimator***, which runs across rows of GM and GD and calculates pixel-based MAE and MSE:

Pseudo-code of the Stripe Noise Estimator:

```
Window Height = K (window is vertical, sliding along columns); SN=Stripe Noise;
SN1 – for MAE (Mean Absolute Estimate); SN2 – for MSE (Mean Squared Estimate)
SN1(1:NROWS,1NCOLS)=0; SN2(1:NROWS,1NCOLS)=0;
SN1ROW(1:NCOLS)=0; SN2ROW(1:NCOLS)=0;
for COL=1:NCOLS
        StartRow = (K+1)/2; EndRow = NROWS-(K-1)/2;
        for ROW=StartRow : EndRow
                Row1=ROW-(K-1)/2; Row2=ROW+(K-1)/2;
                WINDOW=A(Row1:Row2,COL) % K-POINT WINDOW ALONG COLUMN
                AVG=MEAN(WINDOW) % AVG = AVERAGE
                for i=1:K  D1(i)=ABS(WINDOW(i)-AVG); D2(i)=D1(i)^2 ; end
                SN1(ROW,COL)=MEAN(D1); SN2(ROW,COL)=MEAN(D2);
        end;
        SN1ROW(COL)=MEAN(SN1(:, COL)); SN2ROW(COL)=MEAN(SN2(:, COL));
end
MAE=MEAN(SN1ROW(:));  MSE=MEAN(SN2ROW(:)) % AVERAGE ALL COLUMNS
============== end of pseudo-code ==================================
```

The test run using 3,499 data files has shown that the BOASNRA C++ code is robust. All data files were processed without exception. The iterative median filter convergence was achieved reasonably fast given the size of data files (images). Each image is an array of 2030 rows x 1354 columns = 2,748,620 pixels. On the average, the convergence over gradient magnitude was achieved after about 15 iterations (Figure 2.5-1). The histogram in this figure shows that in about 80% of all cases convergence required less than 30 iterations. In about 20% of all cases convergence was not achieved after 30 iterations and was terminated. Yet statistics of residuals shows that any incremental improvements after 30 iterations are very small.

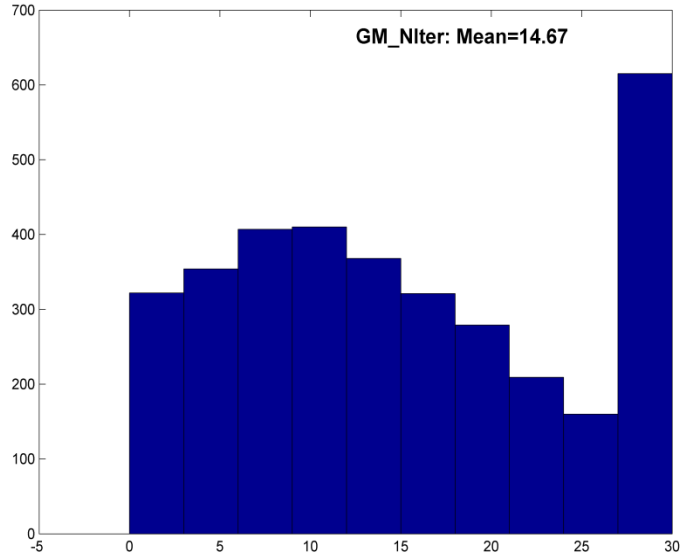

Figure 2.5-1. Number of iterations until convergence for gradient magnitude (mean, 14.67 iterations). The total number of images processed is 3,445. X, number of iterations; Y, number of images.

2.6. Practical Considerations

2.6.1. Numerical Computation Considerations

The BOASNRA is computationally simple. The only computationally intensive operations are:

(1) the contextual adaptive shape-preserving median filter (CASPMF) used in the BOA;
(2) the anisotropic 2D median filter used in the SNRA.

Both median filters are applied repeatedly (iteratively) until convergence. The convergence rate of the CASPMF is relatively fast notwithstanding the structural complexity of the CASPMF. Indeed, the CASPMF is a two-layer *annular filter*, which consists of a 3x3 median filter operating within a larger 5x5 median filter. The larger 5x5 median filter slides across the image while the 3x3 median filter slides across the ambient 5x5 window. The convergence rate of the SNRA is much slower despite its simplicity; however the most substantial improvements (stripe noise reduction) are achieved after the first 10-20 iterations. Nonetheless, our experience has shown that iterative median filters are not computationally demanding, therefore the SNRA is allowed to iterate until convergence or until 300 iterations (whichever comes first). The relatively low computational intensity of the BOASNRA is at least partly accounted for by the high efficiency of numerical sorting implemented in the median filters and also because of the relative small window sizes – 3x3 and 5x5 and 3x5 – used in both median filters.

2.6.2. Programming and Procedural Considerations

The BOASNRA algorithm uses two-dimensional iterative median filters that pass over the same image until convergence. One-dimensional media filters are known to always convergence, to the so-called root signal; moreover, the nature of the root signal is known: this signal is locally monotonous (Gallagher and Wise, 1981). Two-dimensional median filters (2DMF) do not necessarily converge: There is no guarantee of convergence of 2DMF. In some pathological cases, 2DMF may exhibit an oscillatory behavior by switching back and forth between two stable modes. Even though the probability of encountering such pathological cases in real satellite image is likely infinitesimal (such oscillations have not been observed after running the BOASNRA over several thousand of images), we hard-coded a circuit breaker that terminates the iteration process in the SNRA after 300 iterations (see the SNRA flowchart in Fig. 2.3-2). This is a safety precaution that does not affect the quality of the output product. The threshold number (300) far exceeds the typical number of iterations required to achieve substantial improvement of image quality. Our practical experience with MODIS Aqua images shows that image quality improves most significantly after the first few iterations (10 to 20 at most) and that all subsequent improvements are getting progressively less pronounced as the iteration process is going on.

2.6.3. Quality Assessment and Diagnostics

The quality of output frontal maps can be assessed against in situ data and other satellite products (collocated and synchronous). An experienced oceanographer could qualitatively evaluate features displayed in the output products and point out some features that could be artifacts. At the same time, the quality of SNRA can be quantitatively assessed by using three parameters – DIST2, NITER_C, and NPIX – that characterize the improvement achieved owing to SNRA and also the computational cost of SNRA. The best way to monitor these parameters is to tabulate and display DIST2, NITER_C, and NPIX. Accumulation of these data after running the BOASNRA over several thousand images would allow robust statistics to be computed.

2.6.4. Exception Handling

The iterative median filter is known to converge fast. In 1D, median filter always converges. In 2D – and this is our case – there is no theoretical guarantee of convergence. In some pathological cases (=exceptions), iterative median filter applied to an image would oscillate indefinitely between two states. To prevent this from ever happening, a circuit breaker is hard-coded in the SNRA. This circuit breaker stops the iterative median filter automatically after 300 iterations (see the SNRA flowchart in Fig. 2.3-2). Our experience has shown that any improvement (stripe noise reduction) achieved after 300 iterations is insignificant. Therefore, forcing termination of the iteration process does not degrade the output product.

2.7. Validation

2.7.1. Introduction

Testing and validation of the BOASNRA has been done in several steps. First, separate blocks of the BOASNRA have been tested in isolation. After testing each block individually, the entire BOASNRA has been tested and validated as a whole. The most important block, the Belkin-O'Reilly Algorithm (BOA), was initially tested in the Synthetic Image Generation (SIG) environment, and later validated with thousands of real satellite images (Belkin, Hyde, and O'Reilly, 2012) and with *in situ* oceanographic data (Belkin, Melrose, and Hare, 2012). The BOASNRA has been tested and validated with 3,500 MODIS Aqua Ocean Color Level-2 images obtained via the NOAA CLASS system (www.class.noaa.gov). The BOA has also been validated with MODIS Aqua Ocean Color Level-3 data obtained from the NASA Goddard Space Flight Center (http://oceancolor.gsfc.nasa.gov/cgi/l3). Each of these validation sub-projects is described below.

2.7.2. Testing and validation of contextual median filter on model (synthetic) images

Performance of the contextual MF was evaluated on model (synthetic) images (Figs. 2.7-1 through 2.7-3) that capture main spatial features of frontal zones on a variety of scales:
1. Large-scale water mass fronts, e.g. Gulf Stream (100–1000 km).
2. Meso-scale fronts around eddies, especially rings (50–100 km).

3. Meso-to-small-scale fronts around spin-off eddies (*shingles*) that develop on large-scale and meso-scale fronts (10–50 km).
4. Chl enhancement at fronts (Chl ridges).
5. Local Chl blooms (Chl peaks).

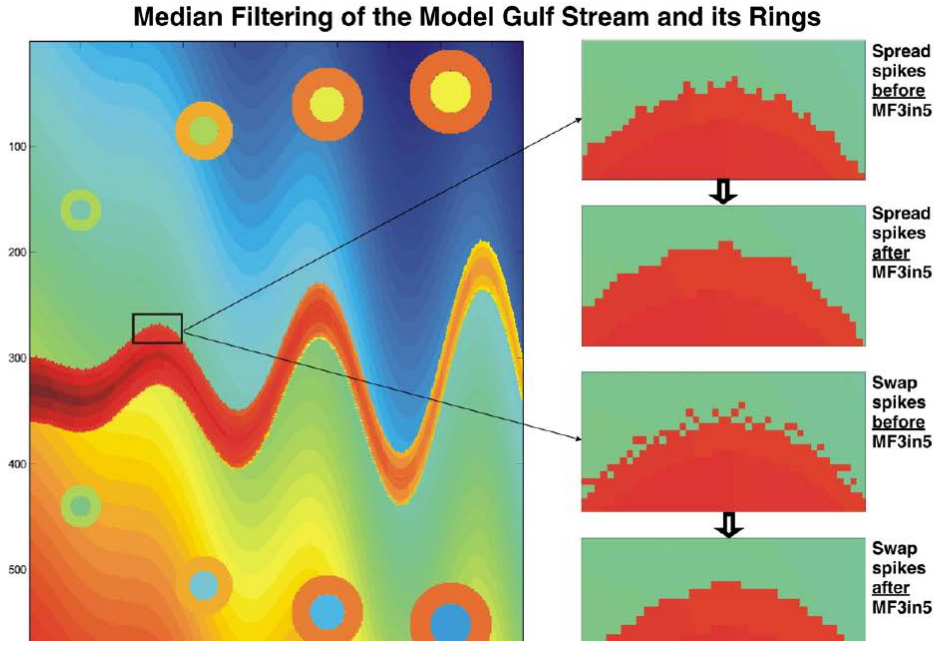

Fig. 2.7-1. Median filtering of the model Gulf Stream and its rings (Belkin and O'Reilly, 2009). The right panel shows two types of spikes and the effect of median filter.

The above features were modeled against spatially varying fields to test the filter's insensitivity to the background. Testing the filter on the widely meandering Gulf Stream (GS hereafter), round-shaped rings and spiral eddies/ridges confirms the filter's rotational invariance. The GS north and south edge ("wall") have been intentionally corrupted by adding 1-point spikes and 3-point spikes that alternate along each edge. To test the algorithm's insensitivity to spike rotation/orientation, meridionally-oriented spikes were added to the north wall, while zonally-oriented spikes were added to the south wall. Two kinds of *horizontal spikes* in xy-plane were used for testing:

(1) Spikes created by *swapping* adjacent pixels. After these spikes are added, the GS edges look frayed.
(2) Spikes created by *spreading* the GS warm pixels outward. After these spikes are added, the GS edges look rugged.

The swap and spread spikes make the model Gulf Stream edges mimic small- and meso-scale shingle-like meanders commonly observed along edges of the real Gulf Stream and other large-scale fronts (Fig. 2.7-1). Rings (Fig. 2.7-1) and spiral eddies-ridges (Fig. 2.7-2) vary in size to test the filter's scale invariance and its insensitivity to feature dilation (scaling transformation). The spiral eddies-ridges also vary in structure: narrow ridges (left column)

are only one pixel across, whereas wide ridges (right column) are three pixels across and have a sharp crest. Chl peaks (blobs) are of three sizes (Fig. 2.7-3): 1-pointers are spikes assumed noise that must be removed, whereas sharp 3-pointers and 5-pointers defined on 3×3 and 5×5 compacts respectively need to be preserved intact. Since the 1-pointers are along z-axis, they are called *vertical spikes*.

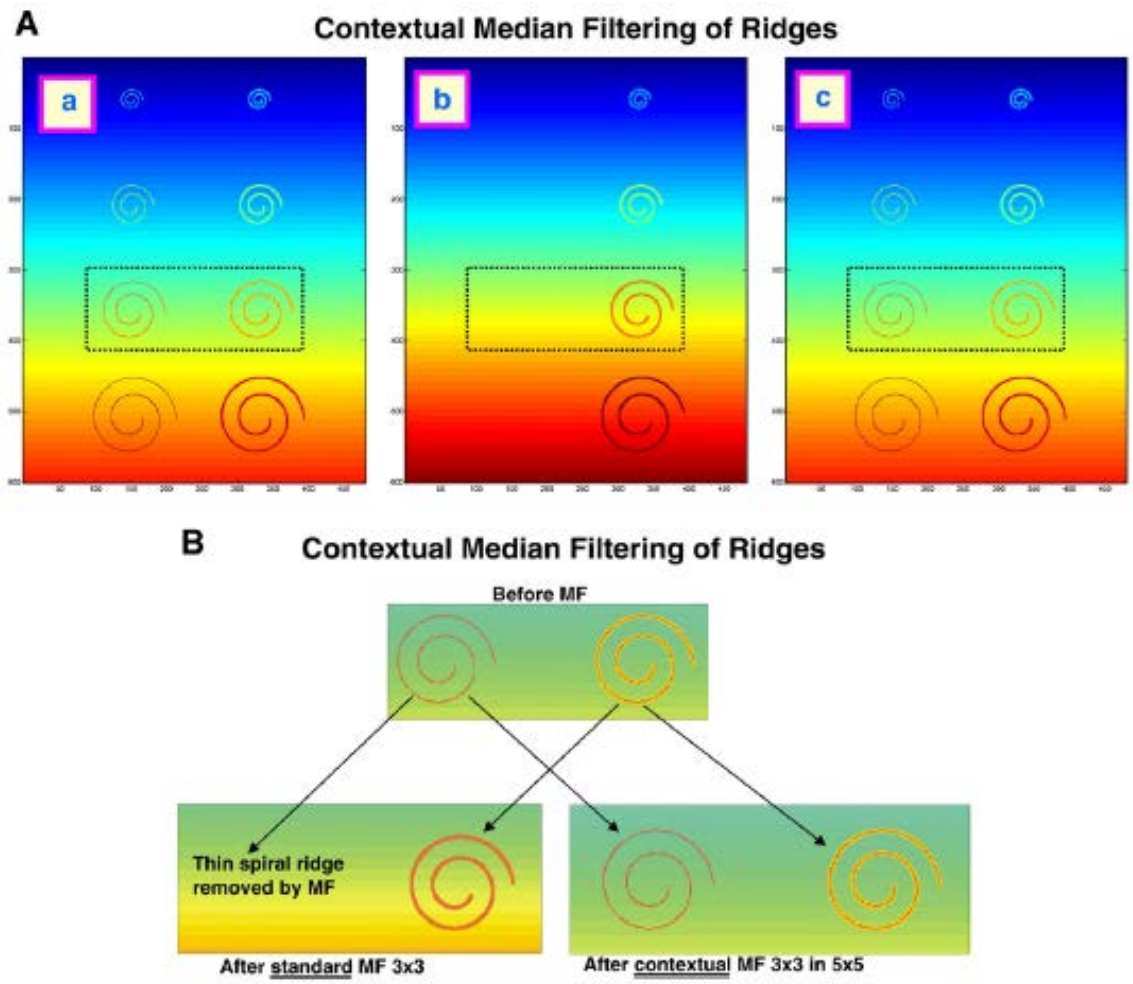

Fig. 2.7-2. Contextual median filtering of ridges or “roof edges” is robust and invariant to the varying background, scale and orientation of these features (Belkin and O’Reilly, 2009).

2.7.3. Validation of front detection algorithm with real satellite images

The BOA was validated with >6,000 images of Chl and SST obtained for the U.S. Northeast in 2002-2011. Climatology of Chl and SST fronts for the U.S. Northeast was compiled based on 10 years of MODIS Aqua data (Belkin, Hyde, and O’Reilly, 2012). These climatologies have been compared to identify collocated features (fronts) observed synchronously. This comparison presents a powerful instrument for cross-validation of the

front detection algorithm (BOA) since Chl fronts are markers of SST fronts. We also validated the BOA by comparing the SST climatology generated by the BOA with a regional climatology of SST fronts generated by the Cayula-Cornillon algorithm (Ullman and Cornillon, 1999, 2001; Belkin, Cornillon, and Sherman, 2009). The main reason for the parallel usage of Chl and SST frontal climatologies was two-fold: (1) Chl fronts are excellent markers of SST fronts, especially in summer when many SST fronts all but disappear after being obliterated by spatially uniform surface warming; (2) Another, independent climatology of SST fronts was previously obtained using the Cayula-Cornillon algorithm (CCA) based on a completely different approach called histogram method (Belkin, Cornillon, and Sherman, 2009). The BOA-generated Chl frontal maps were compared with the collocated CCA-generated maps of SST fronts for the same months. The comparison was made in the following areas: South Atlantic Bight, Mid-Atlantic Bight, Nantucket Shoals, Georges Bank, Gulf of Maine, and Nova Scotian Shelf. The BOA- and CCA-generated maps compare quite favorably. All fronts identified by CCA have been identified by BOA. At the same time, the BOA-generated maps revealed many small-scale and meso-scale fronts that have not been previously reported. The most conspicuous examples are newly-identified fronts over the Nantucket Shoals and Georges Bank. These fronts persist year-round, which can be explained by topographic steering. Spatial gradients associated with these features are quite strong. The bathymetrically-induced stability combined with strong spatial gradients renders these fronts important to fisheries and navigation. Results of this investigation are reported in detail by Belkin, Hyde, and O'Reilly (2012).

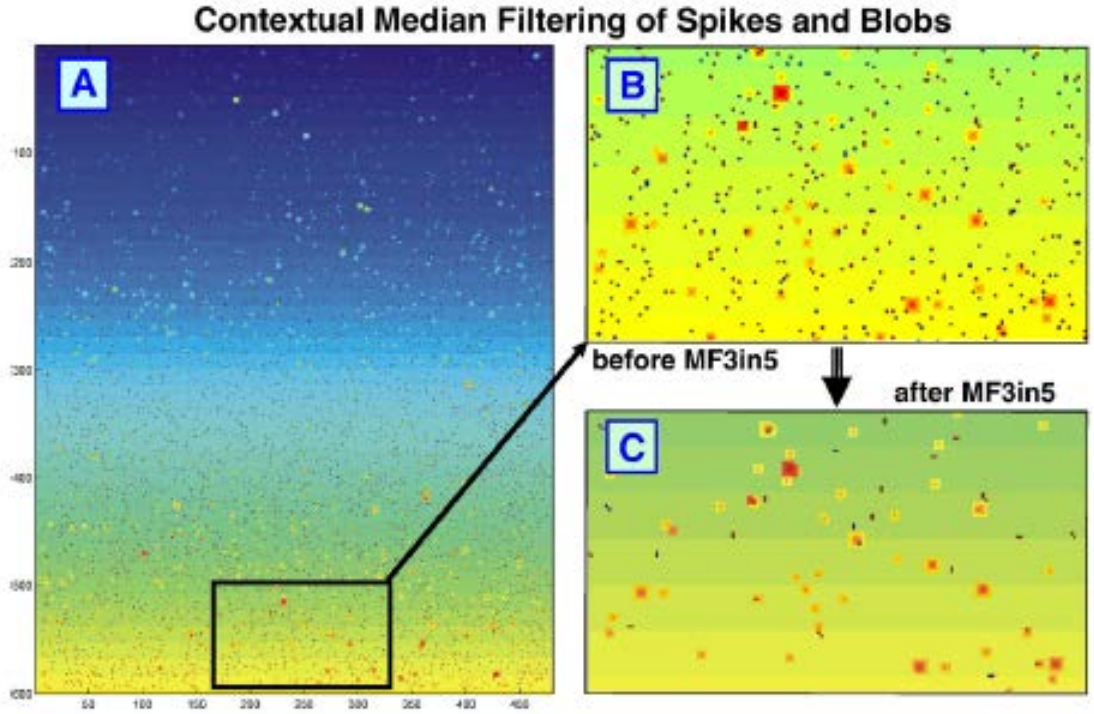

Fig. 2.7-3. Contextual median filtering of spikes and blobs (Belkin and O'Reilly, 2009).

2.7.4. Testing and validation of BOASNRA with instant real satellite images

Screening Test Data Set. The BOASNRA was tested and validated using the Test Data Set (TDS) described in section 2.5. The TDS includes all available MODIS Aqua Ocean Color data from April 1 through May 31, 2012. These data are archived as HDF files at the NOAA's Comprehensive Large Array-data Stewardship System (CLASS, www.class.noaa.gov) maintained by the NODC. The TDS consists of 3,499 files with total volume of >500 GB. The TDS was processed with the BOASNRA C++ code on a dedicated platform described in section 2.5. Since most images are heavily contaminated by clouds, fog, and haze, the TDS was screened to select a subset of ~300 relatively high-quality images (with less clouds); yet another screening was performed, resulting in ~30 best images selected for demonstration purposes as they illustrate various types of fronts observed and successfully detected in geographically and physically diverse regions.

Visualization. Special care was taken in developing customized color scales for Chl, gradient magnitude GM and gradient direction GD. This is not an easy task since each scale is required to be stable since dynamic scaling is not allowed. Additionally, a color scale for gradient direction is required to be continuous to avoid the 0°/360° singularity. In that, direction is radically different from magnitude because direction is a periodic physical quantity, whereas magnitude is not. In all three cases (Chl, GM, and GD), the standard RGB color wheel was implemented into three different color scales, two of them (for Chl and GM) being non-linear (quasi-logarithmic).

Cloudiness and its effect on validation. Visual inspection of the entire TDS (3,499 images) has made apparent vast differences in cloudiness between various regions, which severely impacts front detection. Some regions feature cloud-free conditions (e.g., Gulf of California and western tropical Atlantic off Brazil), whereas other regions are mostly cloudy or foggy (e.g., Gulf of Alaska, Bering Sea, and North Atlantic). It should be noted that any conclusions in this document are based on a two-month data set (April-May) from one year (2012) and therefore are not necessarily representative of other seasons and years. It is well known that cloudiness in just about any geographic region exhibits strong seasonal variability. Also, interannual variations of cloudiness in a particular region may be quite significant; therefore no conclusions are made here about climatological conditions in the regions discussed below. Nonetheless, the above-noted geographic differences in visibility of ocean surface from space are quite dramatic and should be taken into account in any future validation efforts.

Regional ranking based on cloudiness. Based on the visual inspection of TDS, various geographical regions are ranked below from the least cloudy to the most cloudy as follows:

1. Gulf of California (including southern approaches west of Mexico)
2. Western Tropical Atlantic off Brazil (the entire broad coastal zone)
3. Gulf of Mexico
4. Mediterranean Sea (especially the western and central parts)
5. Eastern Tropical Pacific (west of Central America and north of the equator)
6. Eastern Tropical Atlantic (off NW Africa)

7. US West Coast (with strong north-south gradient of cloud frequency)
8. US Southeast (South Atlantic Bight)
9. US Northeast (Mid-Atlantic Bight, Georges Bank and Gulf of Maine)
10. Scotian Shelf and Gulf of St. Lawrence
11. Hawaii
12. Great Lakes
13. Gulf of Alaska
14. Bering Sea
15. Beaufort Sea

Ranking of frontal regions. Any validation effort requires presence of *strong* (with large cross-frontal steps of properties), *intense* (high-gradient), and *persistent* (high-frequency) fronts in a given area. Even though fronts are ubiquitous and can be found in any area of the World Ocean in any season, there are regions with strong, intense, and persistent fronts that consistently show up in satellite imagery. The best examples of such regions are the US Southeast and US Northeast, where the year-round Gulf Stream front features sharp gradients of properties. Other regions might be void of strong, intense, and persistent fronts, for example the western tropical Atlantic off Brazil and waters around the Hawaii. Based on the above-noted key parameters of fronts, namely their strength, intensity and persistence, a short list of the "best" frontal regions is as follows:

1. US Northeast (Gulf Stream, Shelf-Slope Front)
2. US Southeast (Gulf Stream)
3. Gulf of Mexico (Loop Current Front, Shelf-Slope Front, Mid-Shelf Front)
4. US West Coast (especially off California)
5. Gulf of California

Results: Several examples below illustrate the BOASNRA performance across the wide spectrum of ocean fronts created by various physical and biological processes that take place in vastly different oceanographic regions (details in Belkin I.M. et al., Destriping of MODIS Aqua Level 2 imagery, in preparation).

Results: Gulf of Mexico. The BOASNRA performs well on real images as illustrated by Fig. 2.7-4. The first image shows Chl in the Gulf of Mexico. Owing to the vast export of nutrients by the Mississippi River, the near-shore areas feature elevated levels of Chl (although ocean color in these areas is also affected by suspended sediments (silt) and yellow substance ("*gelbstoff*" in German) brought by rivers). Nonetheless, a major Chl front is evident at the boundary of the Mississippi Plume. The front transpires in the gradient magnitude (GM) map as well as in the gradient direction (GD) map. The SNRA works well by reducing stripe noise in both GM and GD. Moreover, the SNRA does not reduce the peak values of GM at the plume front, which is important; actually, the SNRA helps define this front better. Still, some leftover stripes are evident northeast of the Mississippi Delta. The reason for this is the width of these stripes: They are wider than the median filter window in SNRA; therefore they won't be substantially reduced by SNRA. Fortunately, this is a rare case. In the great majority of cases, stripes are narrow (1-2 pixels across), so they

are almost completely eliminated by SNRA. Numerical experiments with SNRA have shown that three iterations of a 2D median filter are enough to substantially reduce striping noise and completely eliminate thin stripes. Another interesting benefit of SNRA manifests in the GD maps where hitherto unknown series of meso-scale quasi-parallel streaks (fronts) have been revealed in some images. These streaks (fronts) feature relatively weak gradients; therefore they are not noticeable in GM maps. These newly-identified patterns deserve a special study.

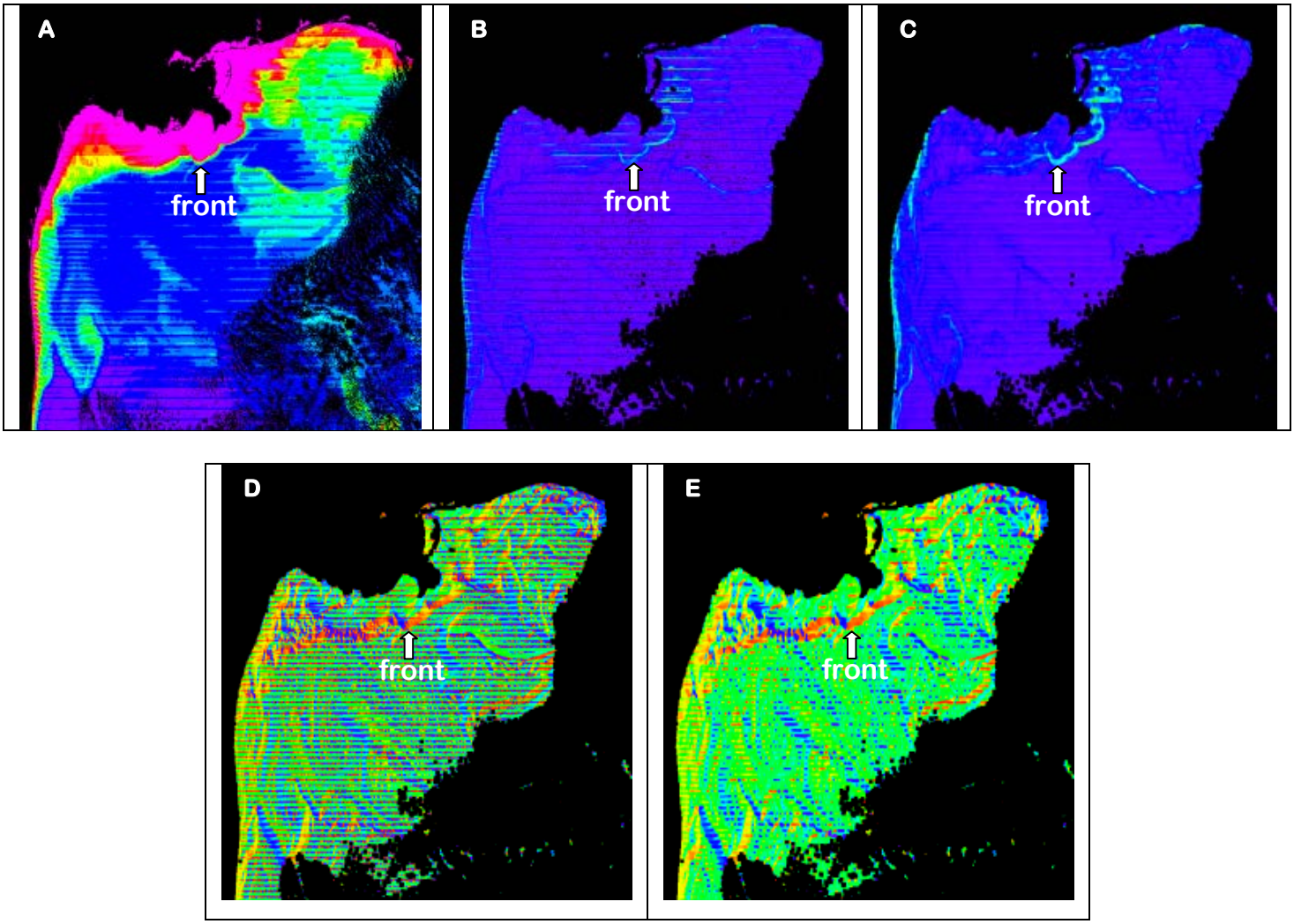

Fig. 2.7-4. Validation of BOASNRA with instant satellite images. (**A**), Chl concentration in the northern part of the Gulf of Mexico off the Mississippi River Delta. **B** and **C,** maps of gradient magnitude before and after SNRA, respectively. Evidently, the SNRA substantially improves the gradient magnitude map quality: the striping pattern is less noticeable and the Mississippi River Plume Front is much better defined in **C** vs. **B**. The same is true with regard to the maps of gradient direction in **D** vs. **E**, respectively.

Results: Gulf Stream fronts in the South Atlantic Bight. Fig. 2.7-5 below shows the Gulf Stream fronts in the South Atlantic Bight (SAB), off the U.S. Southeast coast. The BOASNRA-generated map (right) reveals fine multi-frontal structure of the Gulf Stream as it flows north along the shelf break. It also reveals strong fronts over the SAB shelf.

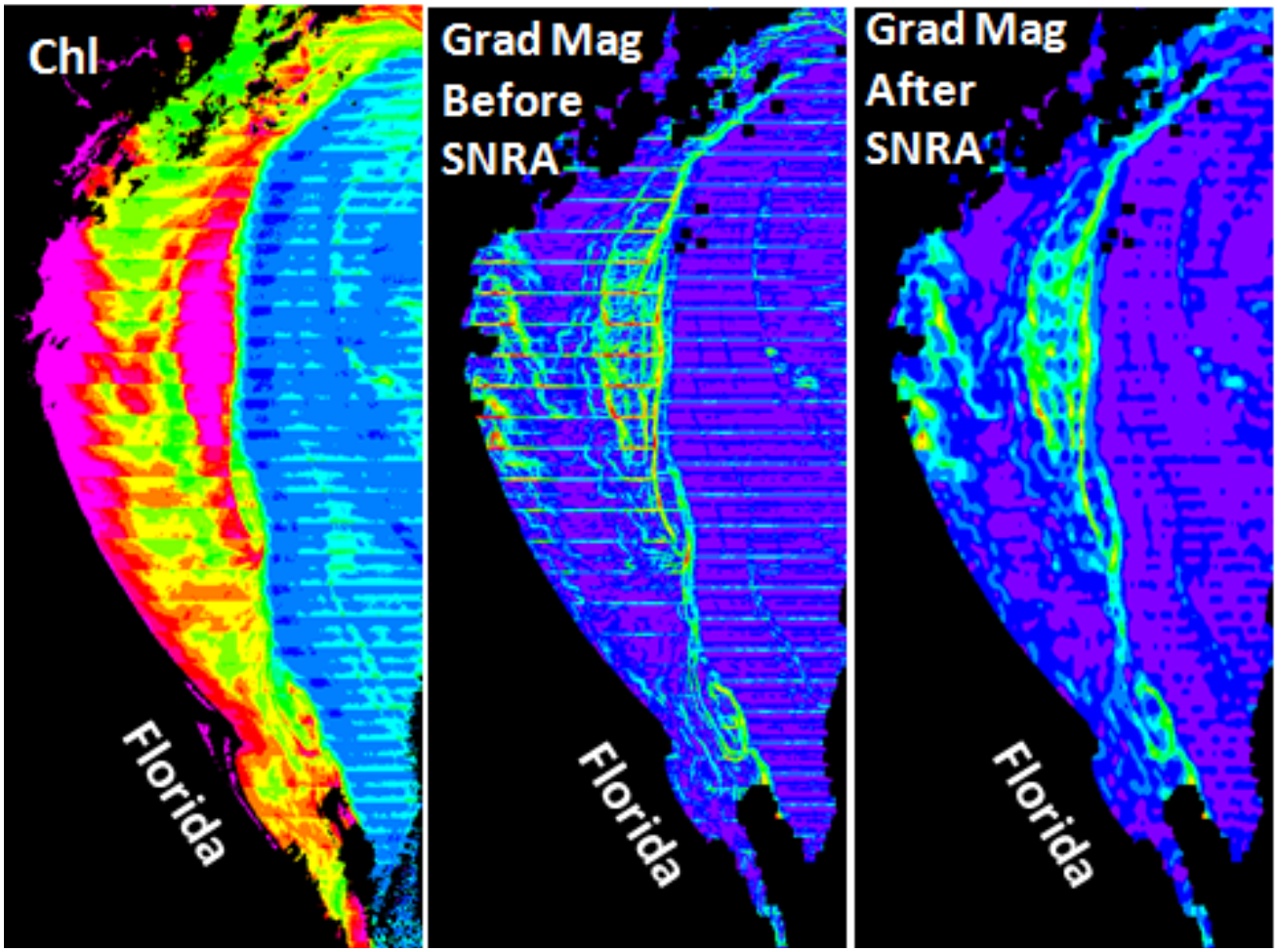

Fig. 2.7-5. Validation of BOASNRA with instant satellite images (cont'd). The leftmost image shows Chl concentration in the South Atlantic Bight off the U.S. Southeast coast. The next two images (center and right) are maps of gradient magnitude before and after SNRA, respectively. Evidently, the SNRA substantially improves the gradient magnitude map quality: the striping pattern is less noticeable and the Gulf Stream fronts are much better defined after SNRA.

Results: Mid-Atlantic Bight. Fig. 2.7-6 shows the Gulf Stream front and warm ring in the Mid-Atlantic Bight off the U.S. Northeast coast. The BOASNRA significantly improves definition (visibility) of various fronts (e.g., compare bottom right vs. bottom left images).

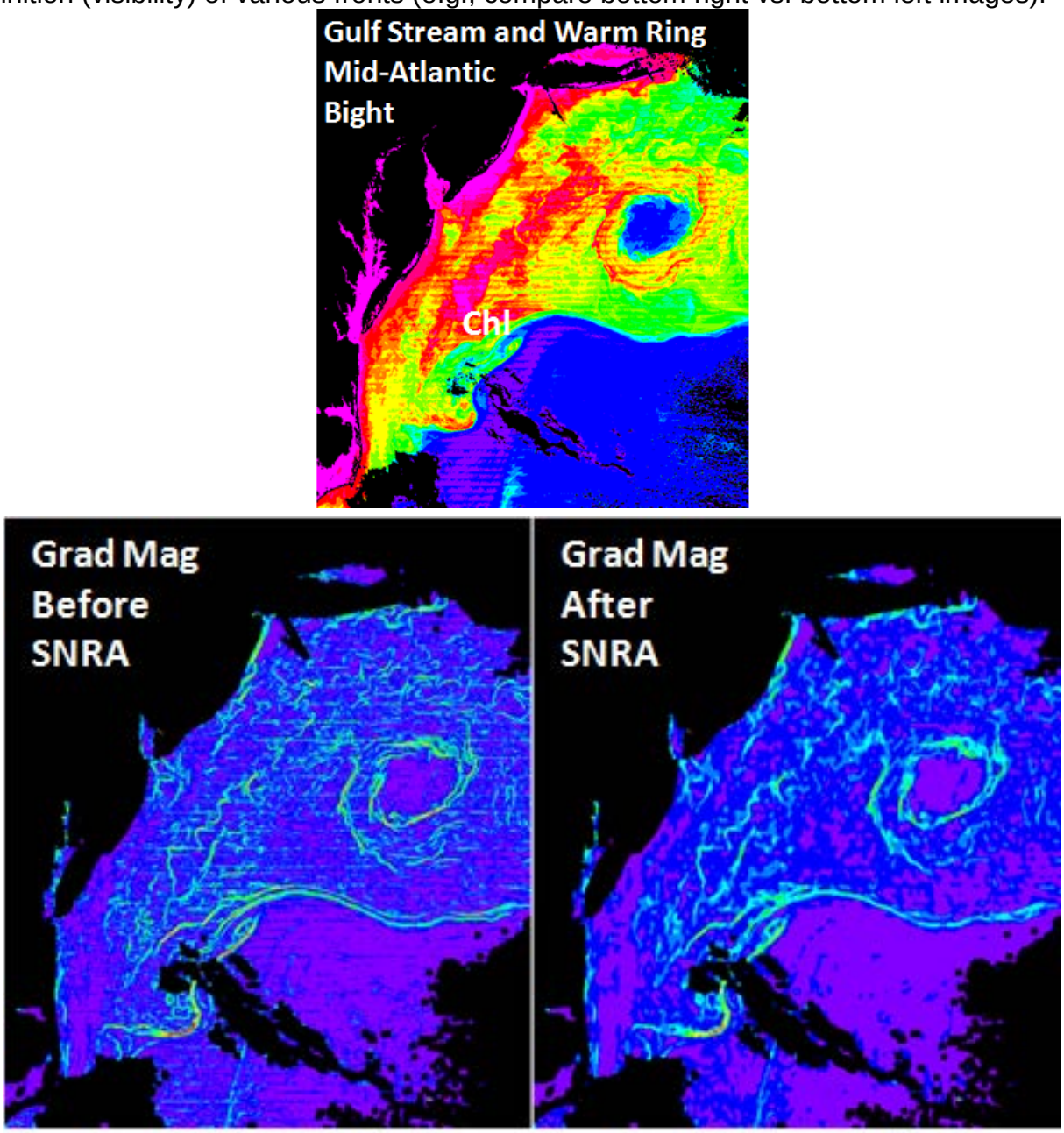

Fig. 2.7-6. Validation of BOASNRA with instant satellite images (cont'd). Top: Chl concentration. Bottom: GradMag before and after SNRA, respectively. The SNRA substantially improves the gradient magnitude map quality: the striping pattern is less noticeable and various fronts are much better defined after SNRA.

2.7.5. Validation of front detection algorithm with monthly satellite imagery

Introduction. Generally speaking, any front detector should be applied to *instant* satellite images, not to *averaged* data, for any averaging tends to smooth fronts. Hence, any climatology of fronts should be generated by (1) running front detector over instant satellite images and then (2) averaging (or compositing) frontal maps obtained during step 1. This principle has been implemented, e.g., at the University of Rhode Island where the Cayula-Cornillon algorithm was developed and used during a global survey of World Ocean fronts (Belkin et al., 2009). Yet *time-domain averaging* (= *temporal averaging*) of satellite imagery of the World Ocean has at least one major advantage, A1: It greatly reduces contamination by clouds. The reason is simple: Clouds move constantly, and even slow-moving clouds move much faster than fronts and eddies in the ocean. There are at least two other advantages of temporal averaging, namely, A2: It eliminates speckle noise, and A3: In case of MODIS Aqua, it greatly reduces stripe noise. In both cases, the noise reduction/elimination is achieved owing to the stochastic nature of speckle noise and stripe noise. Thus, the combination of three advantages, A1+A2+A3, makes temporal averaging attractive in satellite remote sensing and ocean front detection.

Optimum time scale of temporal averaging. When temporal averaging is applied to ocean front detection, the most important question is this: What is the optimum time scale of temporal averaging? In front detection (and image processing in general) there is always a trade-off between noise reduction and feature preservation. By increasing time scale of temporal averaging, noise (both speckles and stripes) can be reduced dramatically to the point of elimination. Yet the time scale of temporal averaging cannot be increased infinitely without significant distortion of frontal pattern. Indeed, most fronts wax and wane on a variety of scales, the most important scale being seasonal. As the season progresses, such fronts emerge and disappear, or migrate back and forth, or change their strength and intensity (cross-frontal range and maximum gradient, respectively), and they often exhibit all three kinds of variability at the same time. Therefore the longest time scale of temporal averaging should be at least several times shorter than the length of a season. Even though seasons in the ocean might have different length depending strongly on location, the average season length is commonly assumed to be 3 months. Therefore the maximum time scale of temporal averaging should be close to 1 month. A visual inspection of bi-monthly maps of Chl routinely made available by the NOAA CoastWatch provides ample empirical justification for the one-month cutoff. The next question to answer is: What is the minimum time scale of temporal averaging? The NASA Goddard Space Flight Center's Ocean Color Web site (http://oceancolor.gsfc.nasa.gov/cgi/l3) has an archive of Chl maps generated for different time intervals, namely 1 day, 8 days and 1 month. Again, a careful visual inspection of all three data sets has shown that daily and 8-day maps are too contaminated by clouds, whereas monthly maps are often nearly cloud-free and reveal frontal patterns quite well. Therefore, based on the above visual inspections of daily, weekly, monthly and bi-monthly maps, *the one-month time scale of temporal averaging was found to be optimum for front detector validation.*

Data. Monthly maps of Chl, January through December 2012 were made for all 9 frontal product CoastWatch areas (**Table 1**). These maps were extracted from respective monthly global fields (Level 3 data) with 4-km resolution downloaded from the NASA Goddard Space Flight Center's Ocean Color Web site (http://oceancolor.gsfc.nasa.gov/cgi/l3). The main goal of this validation effort was to determine if front detection can be performed on monthly Chl maps, rather than instant images. It was necessary to cover as many physically and biologically diverse regions as possible because fronts exhibit tremendous spatial variability around the globe. Fortunately, the 9 frontal product CoastWatch regions cover a vast variety of diverse fronts. Taken together, these regions are quite representative of the entire World Ocean. The above-described data set covers all seasons but is limited to one particular year, 2012. The choice of a particular year is non-consequential since (1) the inter-annual variability of ocean fronts is approximately an order of magnitude smaller than the seasonal variability of the same fronts, and (2) the main focus here is on seasonal (hence 12 months) and spatial (hence 9 regions) variability of fronts.

Table 1. Boundaries of Nine Frontal Product CoastWatch Regions*

*Courtesy NOAA CoastWatch; prefix numbers added to facilitate sorting

Region	W. Lon	E. Lon	N. Lat	S. Lat
1_Northeast	-82	-60	46	30
2_Southeast	-88	-72	37	22
3_Caribbean	-80	-60	30	8
4_Gulf of Mexico	-99	-79	31	17
5_Great Lakes	-93	-75	51	38
6_West Coast	-142	-112	51	29
7_Eastern Tropical Pacific	-142	-80	30	8
8_Alaska	-180	-126	64	50
9_Hawaii	-167	-147	29	10

Results. Each region is represented by two maps: Chl and Chl Gradient Magnitude (GM). Even though maps of Chl Gradient Direction are always generated as a standard product, these maps are less informative here and therefore are not shown. For each region, a single month is chosen subjectively and shown as the "best" month based on the richness and clarity of the monthly regional frontal pattern.

Overall, out of the 9 CoastWatch regions processed and presented here, 5 regions stand out: #1 Northeast, #2 Southeast, #4 Gulf of Mexico, #6 West Coast and #7 Eastern Tropical Pacific. These regions feature strong, robust fronts that are either persistent year-around (e.g., Gulf Stream) or seasonally persistent (e.g., Mid-Shelf Front and Shelf-Slope Front that are strong in winter and fall, respectively, becoming much weaker in other seasons). Region #3 Caribbean has few fronts except of numerous coastal fronts off Venezuela and Columbia. Region #5 Great Lakes features small-scale fronts that require high-resolution

data for detection and mapping. Region #8 Alaska is extremely cloudy; yet strong fronts are visible along the Alaskan Coastal Current and Alaskan Stream. Region #9 Hawaii is the only region void of stable (quasi-stationary) fronts.

Region 1: Northeast

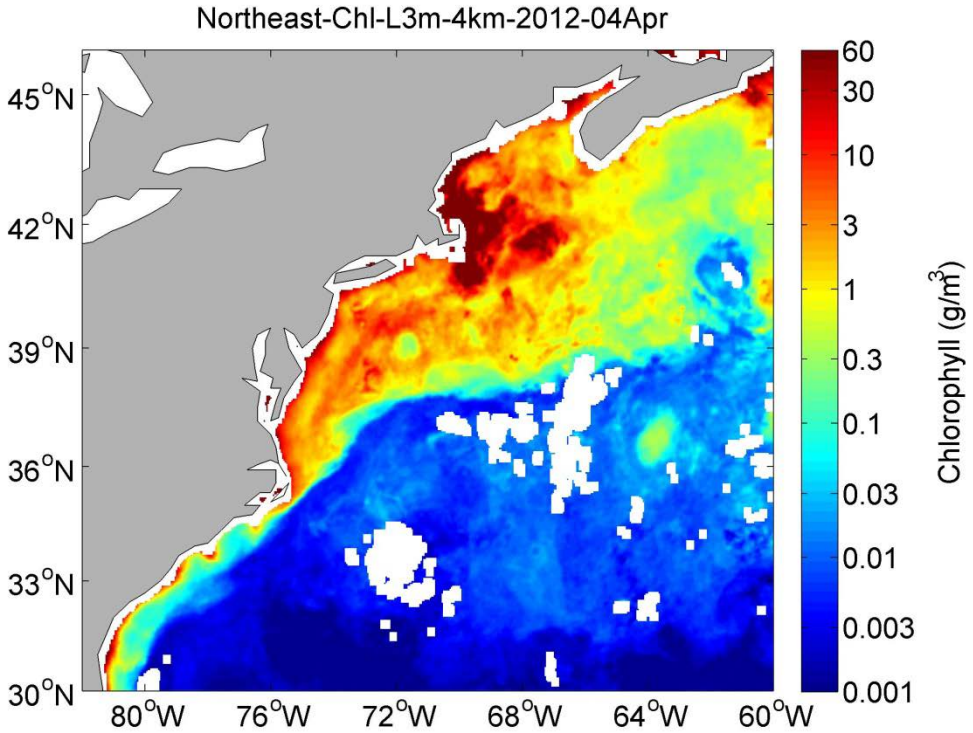

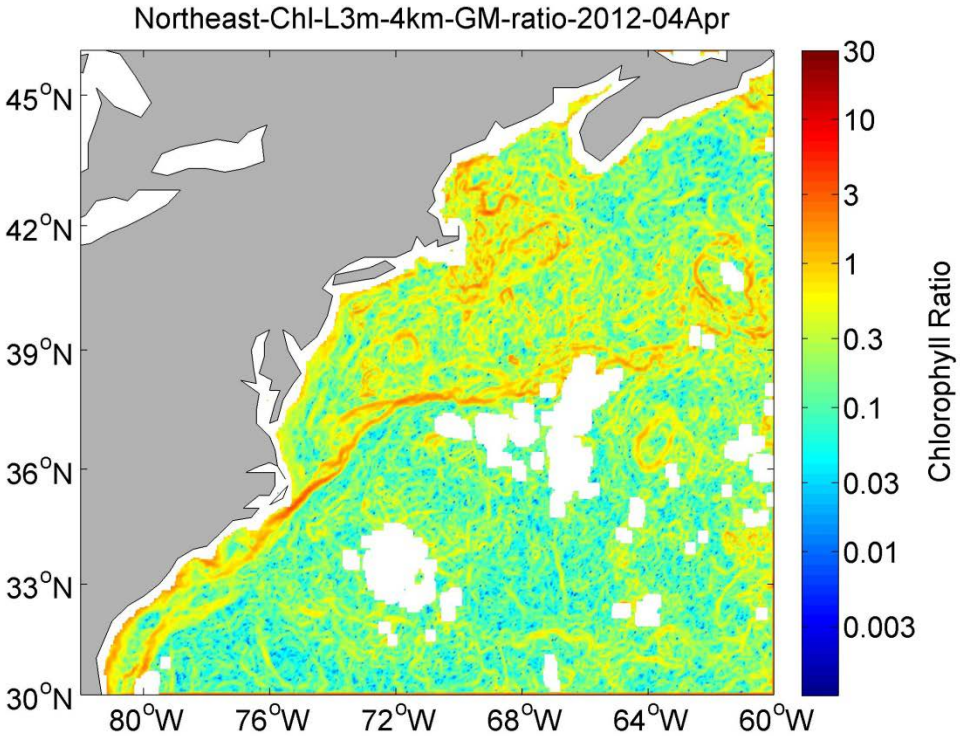

Region 2: Southeast

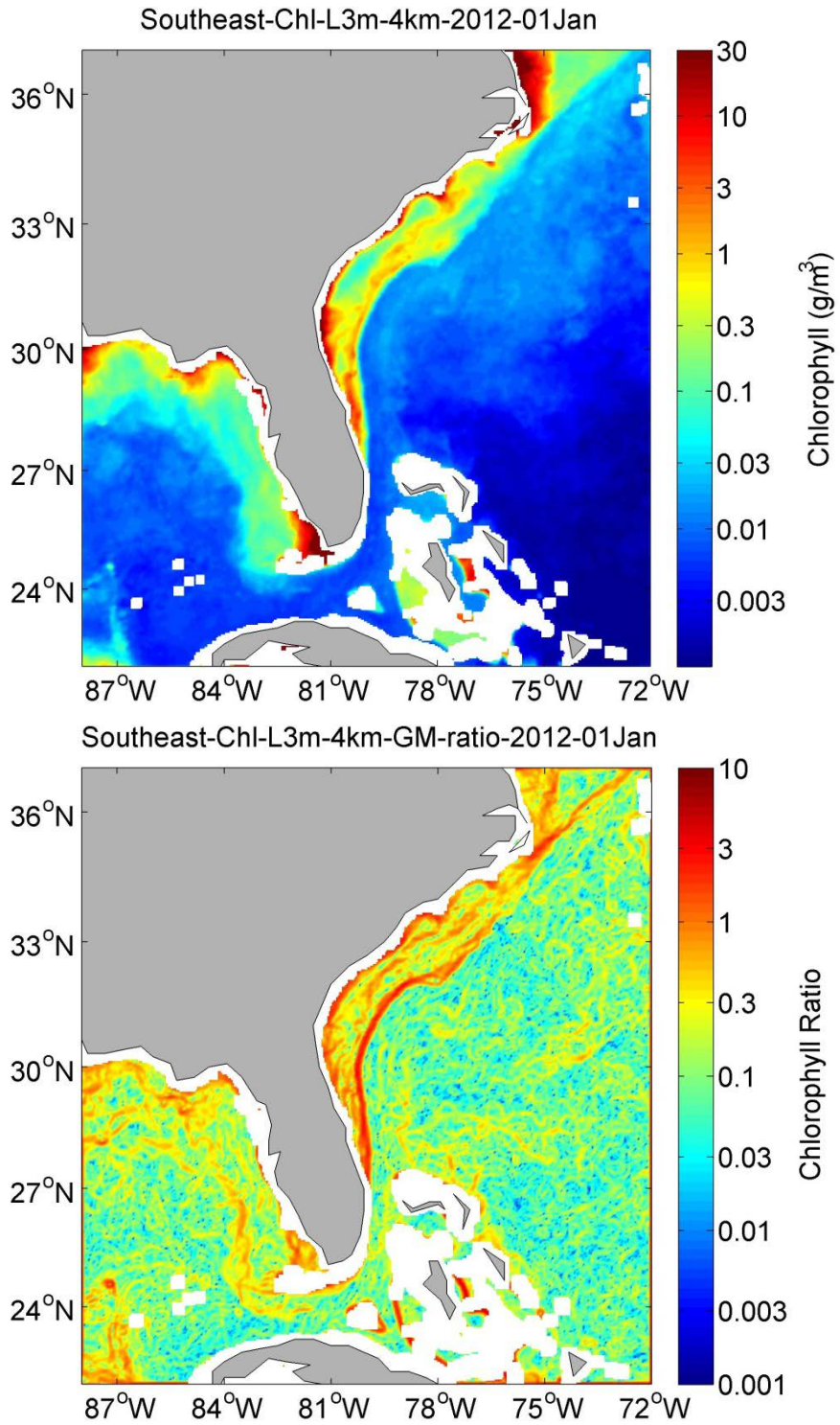

Region 3: Caribbean

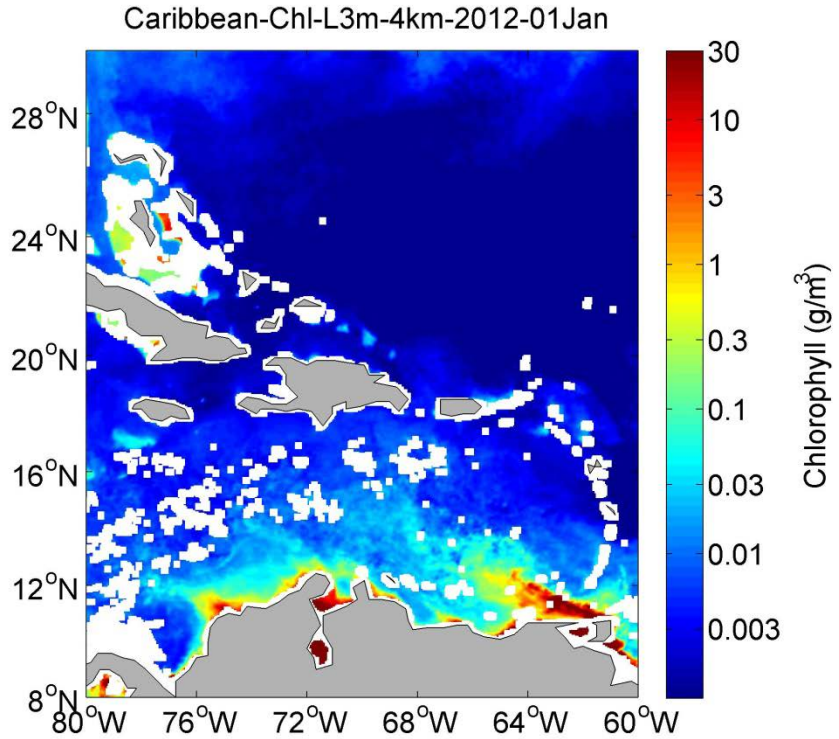

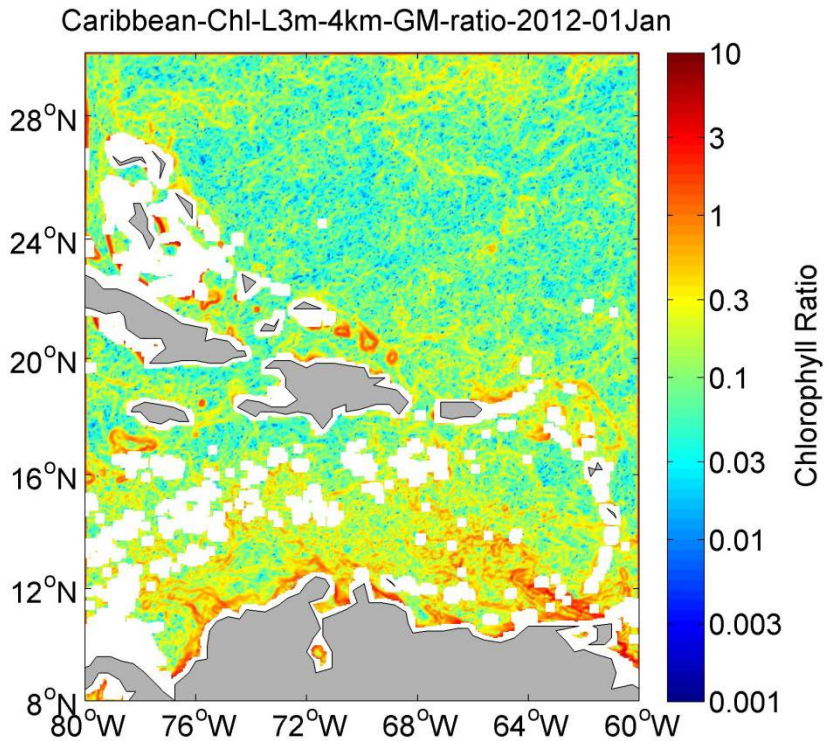

Region 4: Gulf of Mexico

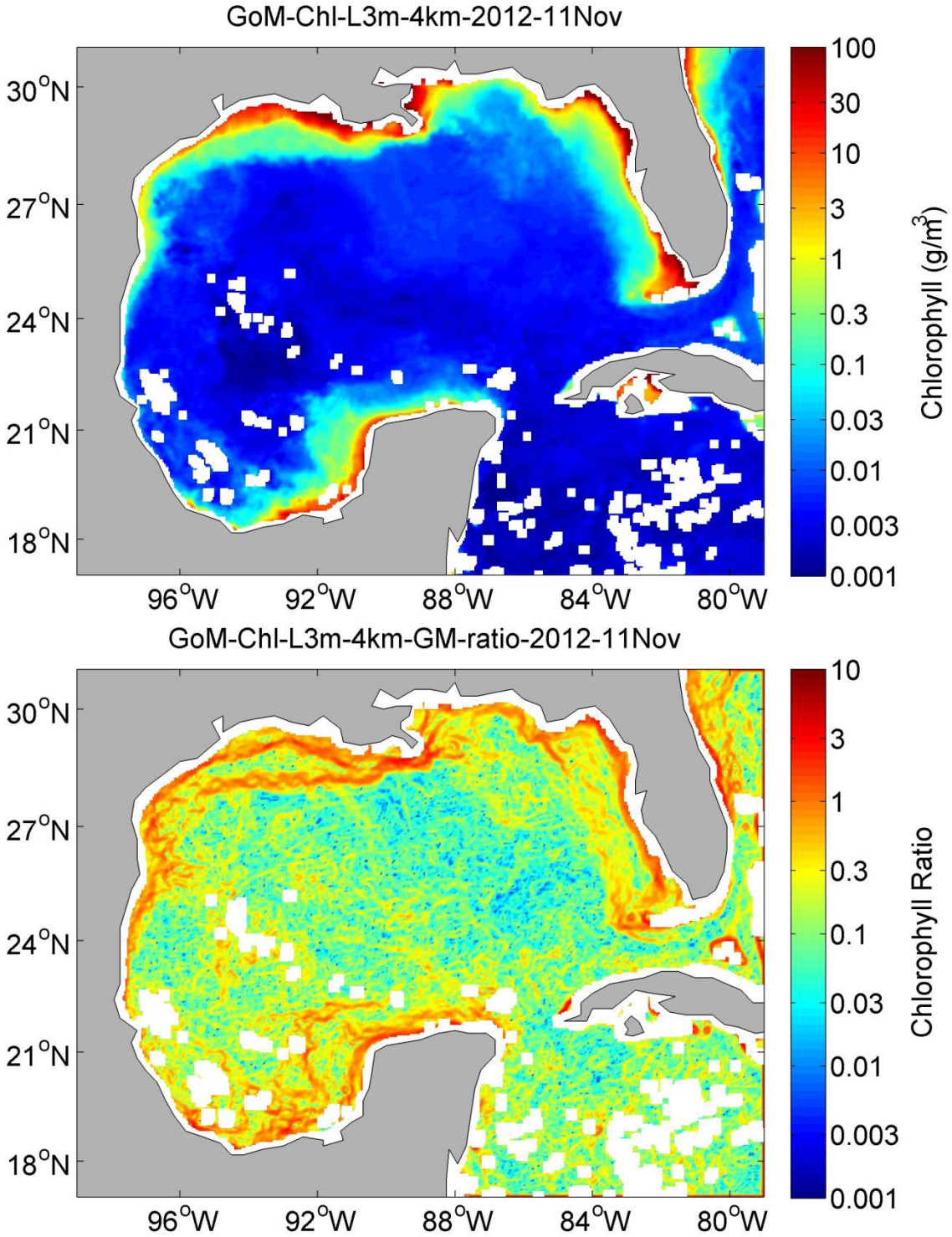

Region 5: Great Lakes

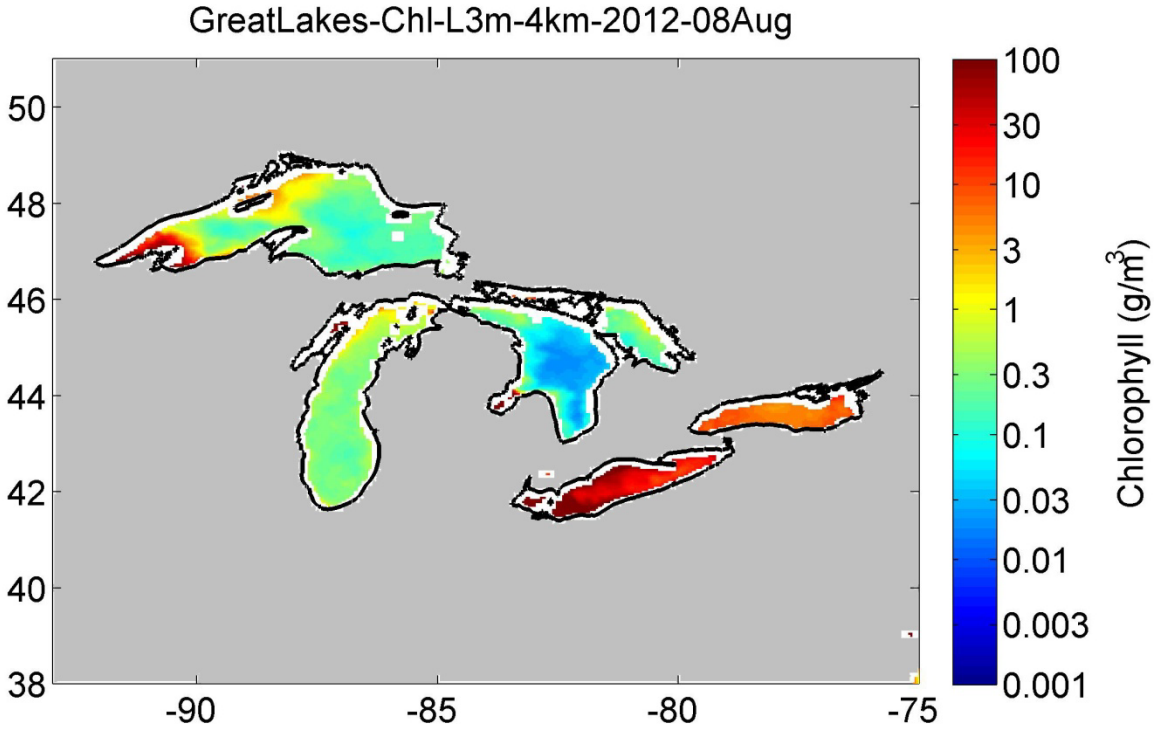

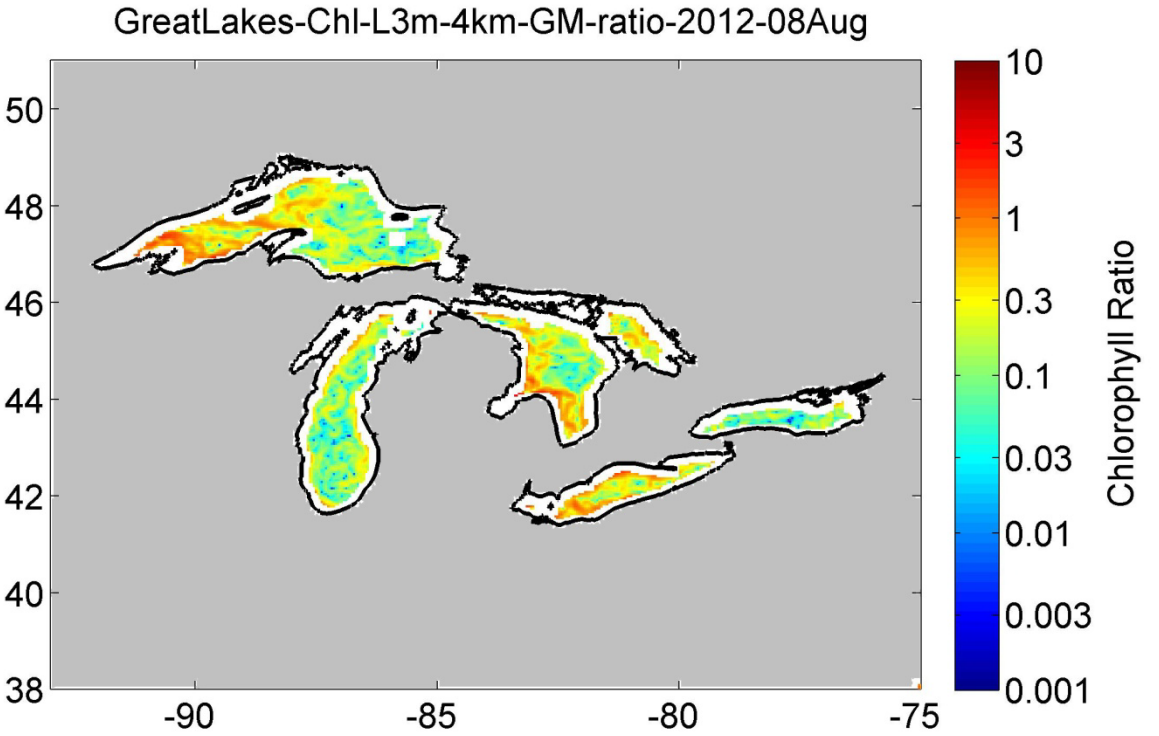

Region 6: West Coast

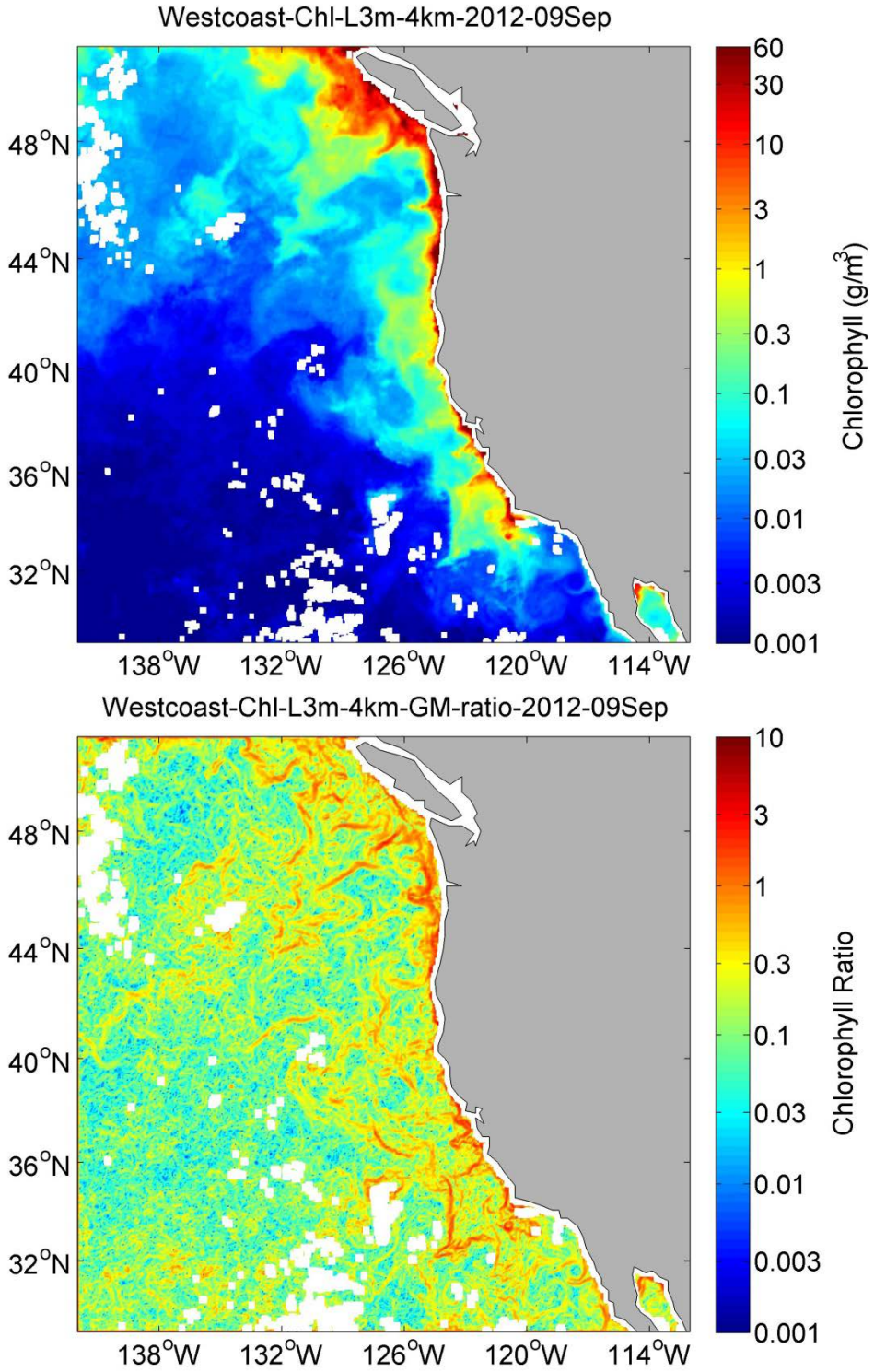

Region 7: Equatorial Tropical Pacific

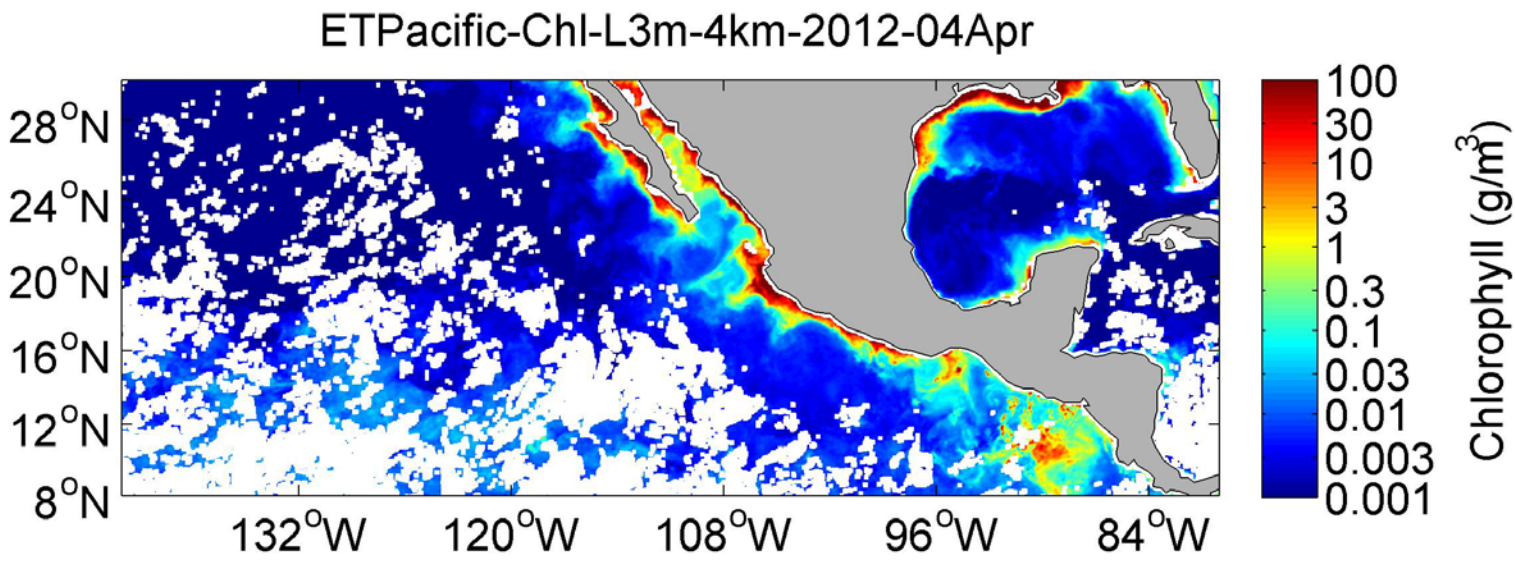

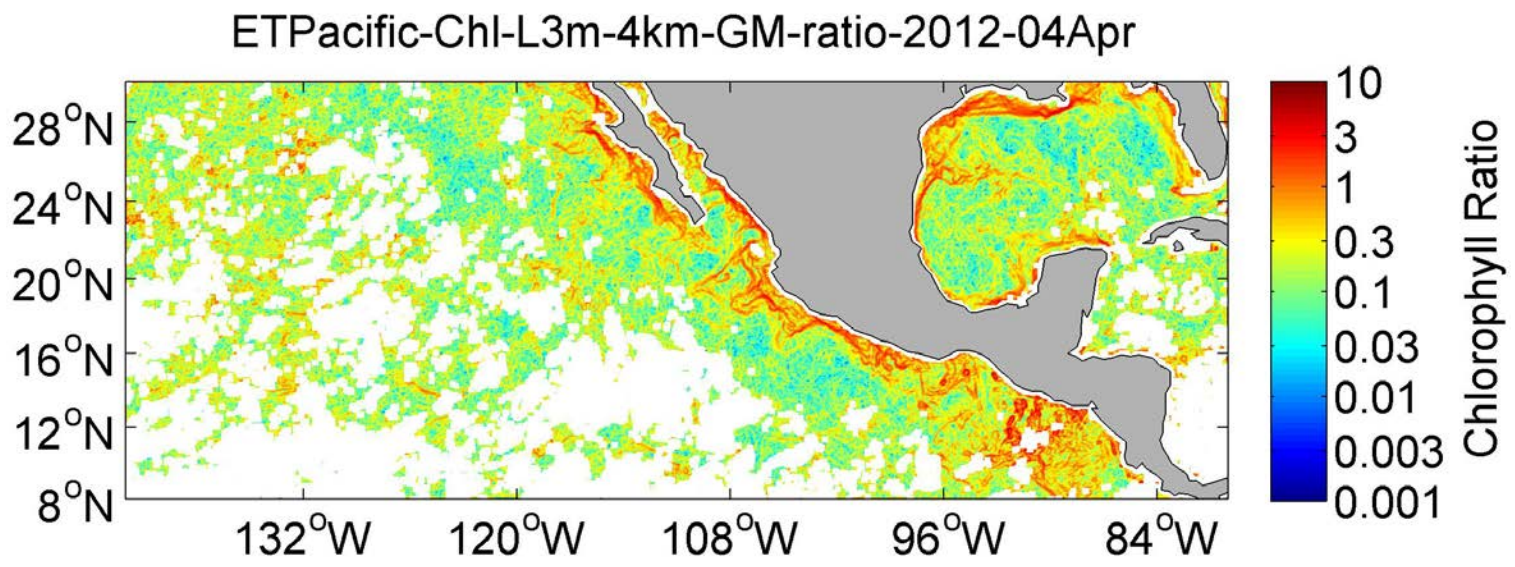

Region 8: Alaska

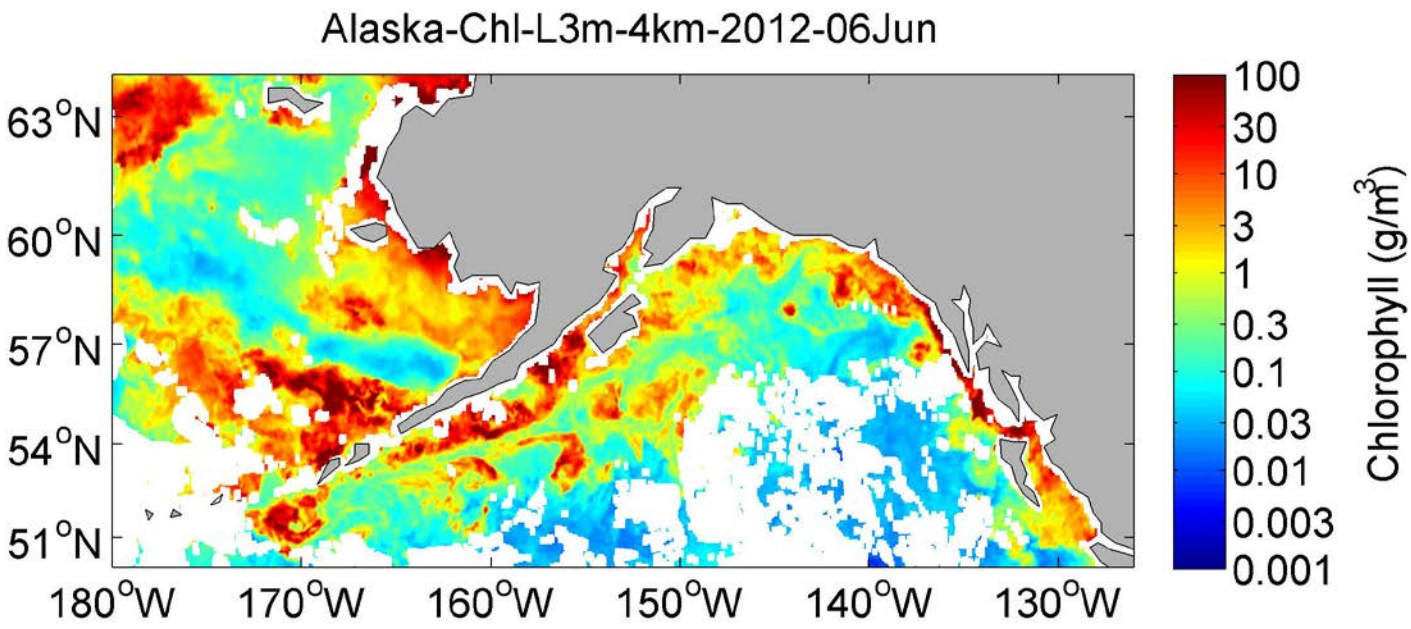

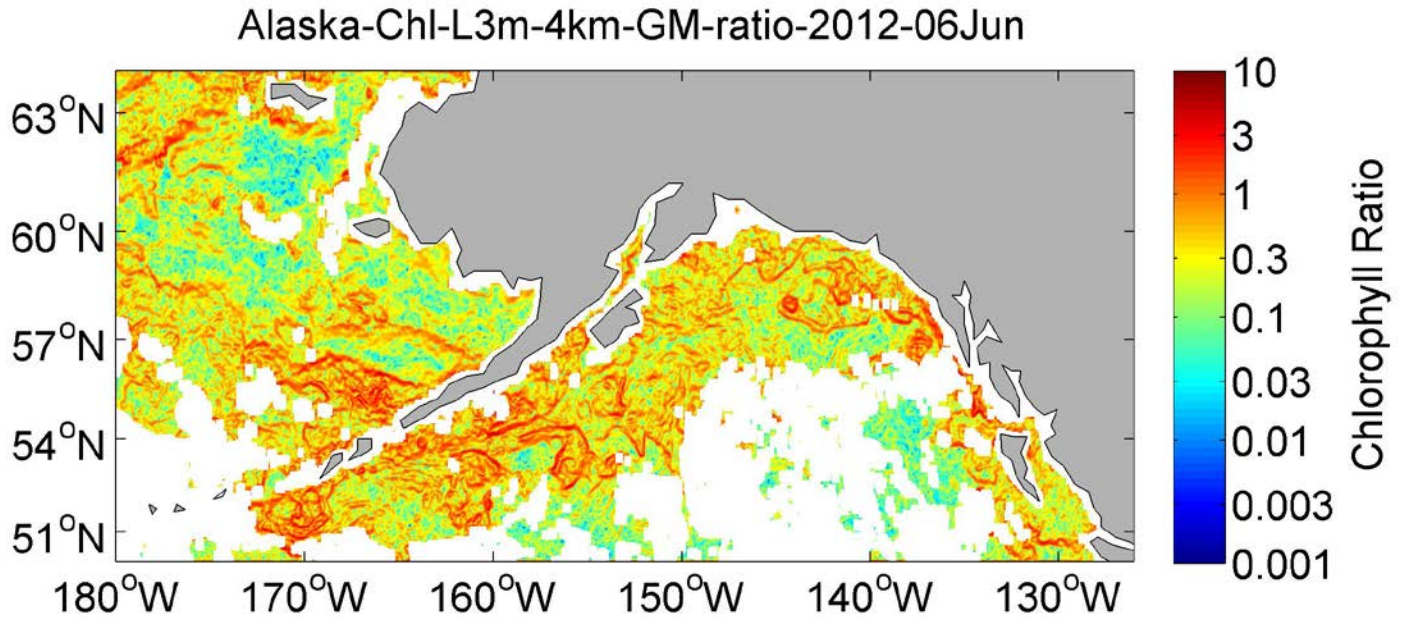

Region 9: Hawaii

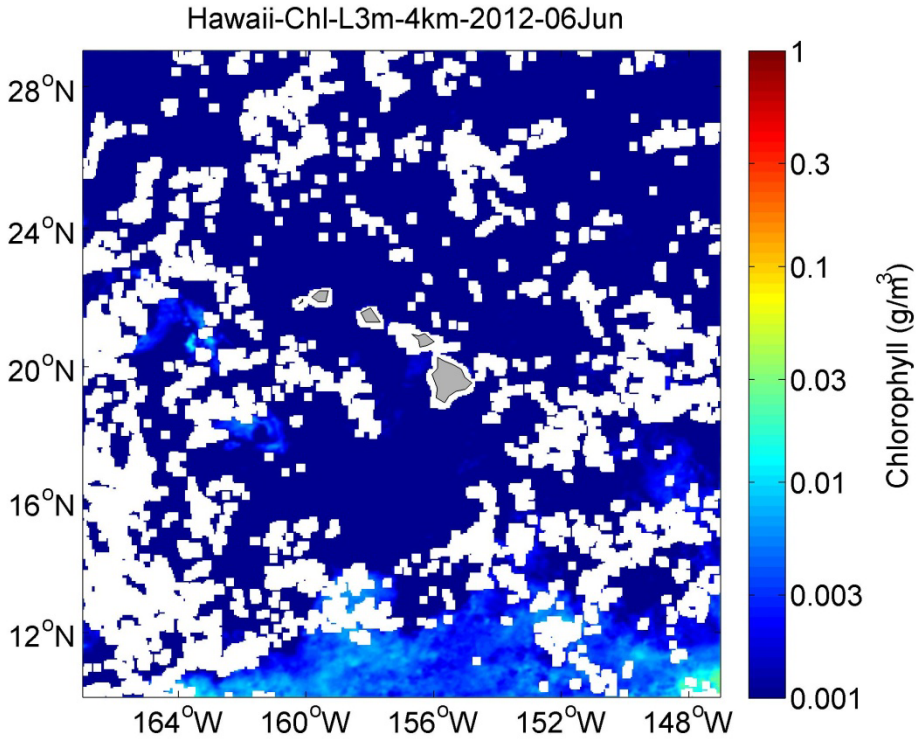

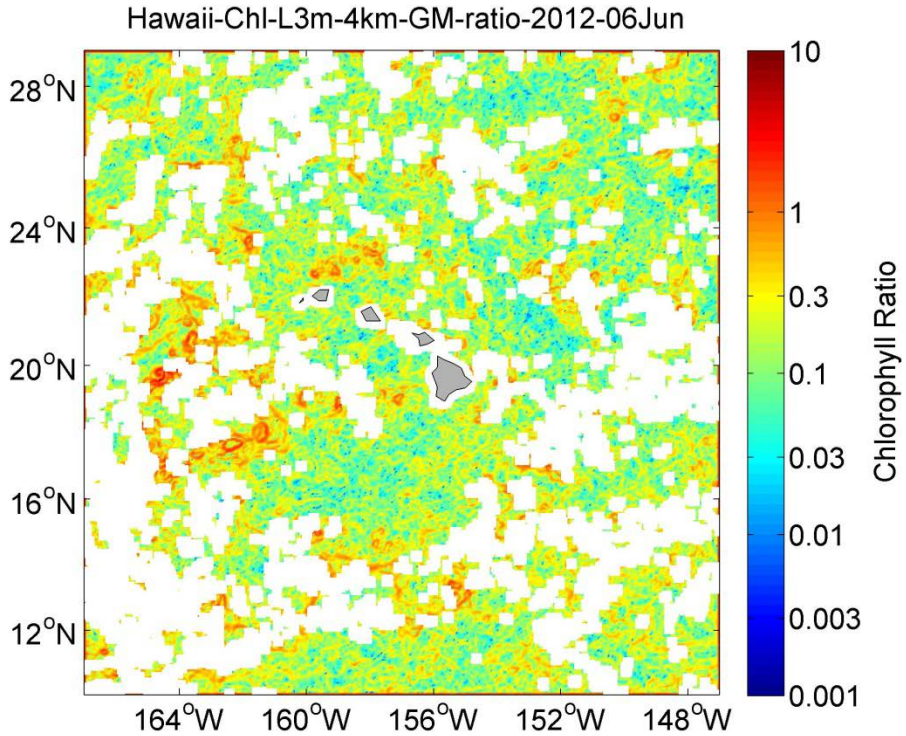

2.7.6. Validation of front detection algorithm with *in situ* data

The *in situ* data set used to validate this front detection algorithm has been collected in the ECOMON cruises conducted by the Narragansett Laboratory, Northeast Fisheries Science Center, National Marine Fisheries Service. The regular seasonal ECOMON cruises covered a large part of the western North Atlantic area within the U.S. Exclusive Economic Zone, including the Gulf of Maine, Georges Bank, Nantucket Shoals, and Mid-Atlantic Bight down to Cape Hatteras (Fig. 2.7-5). This data set was acquired in 25 ECOMON cruises between August 2000 and February 2010. To our best knowledge, no other front detection algorithm has ever been tested on such a large *in situ* data set. During each cruise, up to 20 environmental parameters have been recorded continuously underway, including SST, SSS, and fluorescence, the latter being a proxy for Chl concentration. Fronts in Chl, SST, and SSS are automatically detected in continuous underway data using the software package developed by I.M. Belkin for this purpose. An example of a well-defined front in underway ship-borne SST data is shown in Fig. 2.7-6. All *in situ* fronts are mapped, mutually compared, and quality controlled. After that, the *in situ* fronts are compared with collocated contemporaneous fronts detected by the front detection algorithm in MODIS Aqua imagery. Details of validation with the ECOMON data are to be published as a peer-reviewed paper (Belkin, I.M., Melrose, C., Hare, J., 2012, Validation of a front detection algorithm with in situ underway data, in preparation).

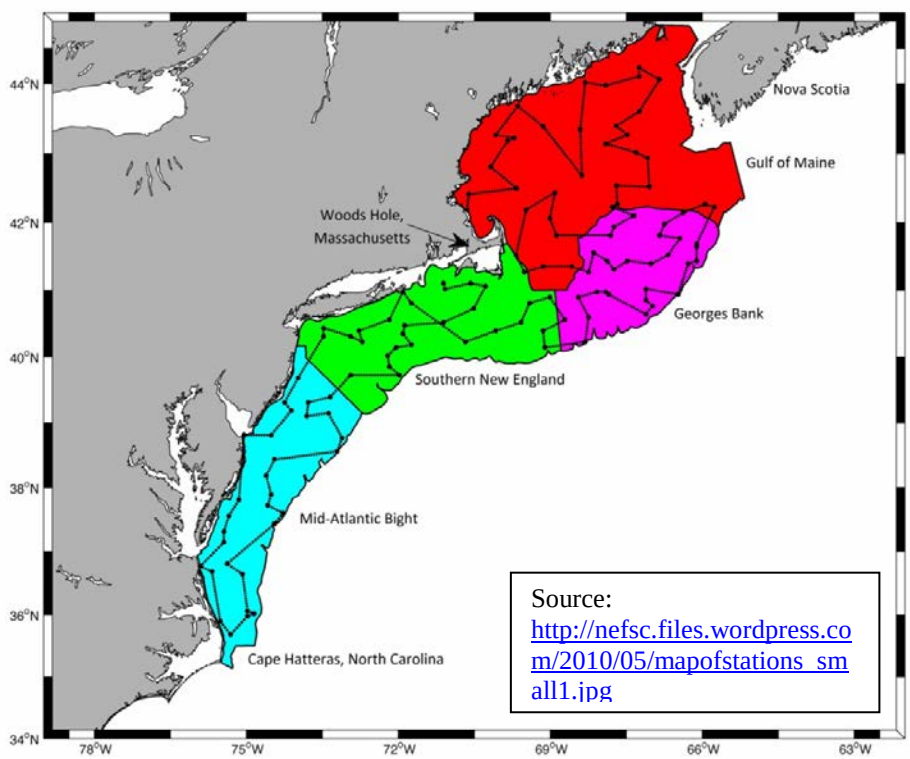

Fig. 2.7-5. ECOMON cruise station map.

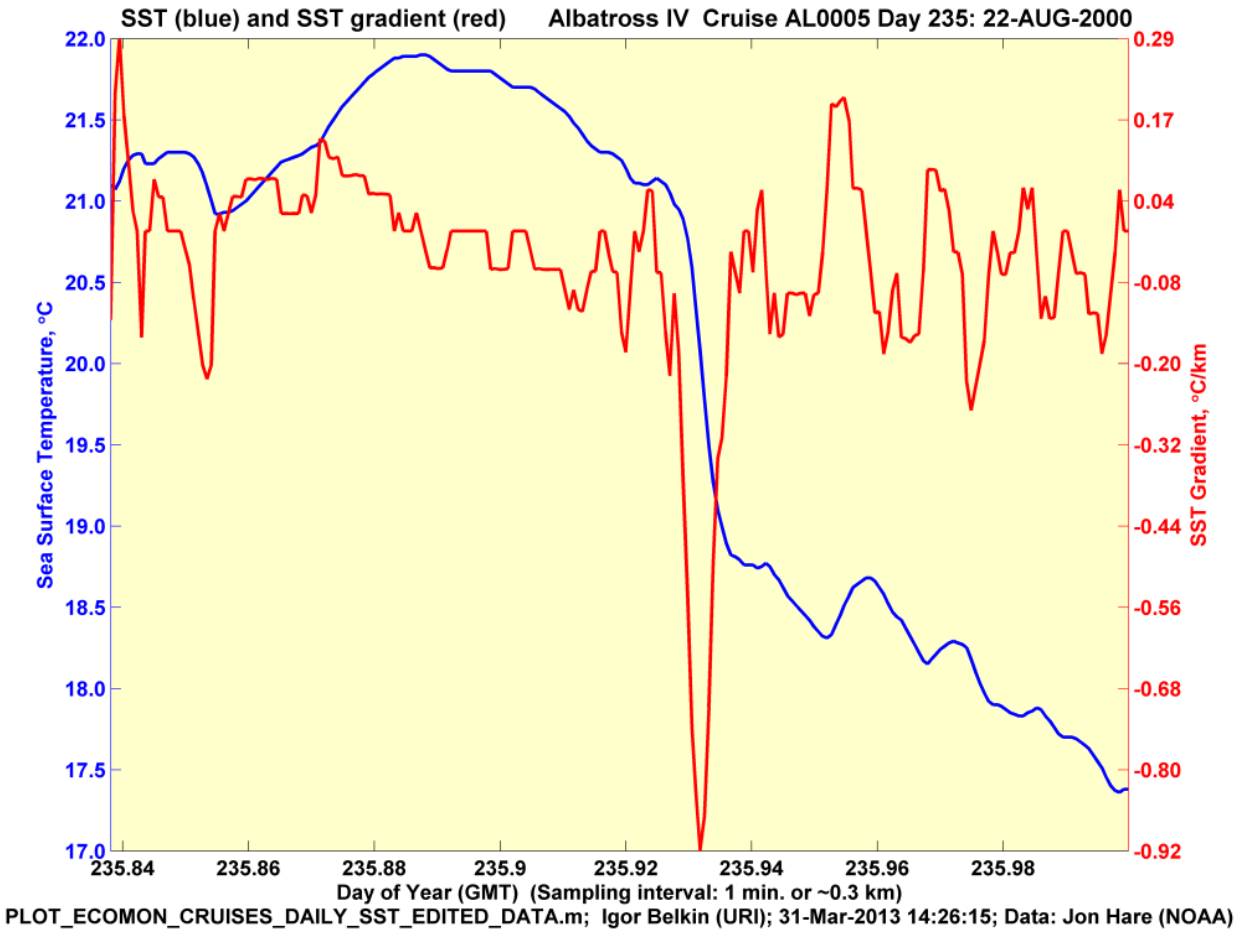

Fig. 2.7-6. Underway ship-borne SST transect across a front.
R/V *Albatross IV* Cruise AL0005, 22 August 2000. Data: Jon Hare (NOAA).

3. ASSUMPTIONS AND LIMITATIONS

3.1. Performance Assumptions

The BOASNRA is designed with no explicit assumptions or models about the input. Yet two notes are warranted:

(1) While designing the contextual adaptive shape-preserving median filter (CASPMF), which constitutes the BOA's core, an assumption was made that all 2D extrema with a single pixel footprint have to be eliminated by the CASPMF since such extrema are considered to be impulse noise. No such assumption was made in the SNRA.

(2) Even though iterative median filter always converges when applied to real satellite images (no oscillatory behavior has been observed so far), the SNRA does not make this assumption and stops the iteration process either after achieving complete convergence or after 300 iterations, whichever comes first (see the SNRA flowchart in Fig. 2.3-2).

3.2. Potential Improvements

(1) Certain improvements in the output product quality and computational efficiency could be achieved by using *recursive* median filters as opposed to the standard (non-recursive) median filters. Recursive median filters have been shown to improve the quality of two-dimensional images (Qia, 1996; Stork, 2003). Currently, the BOASNRA uses non-recursive (standard) median filter.

(2) The BOASNRA has been validated using satellite climatology of Chl and SST fronts in the western North Atlantic (Hyde, O'Reilly, and Belkin, 2008; Belkin, Hyde, and O'Reilly, 2012). Currently the BOASNRA is being validated using *in situ* oceanographic data obtained off the U.S. Northeast. Other potential validation regions can be considered such as the Gulf of Mexico, U.S. West Coast, Alaskan Seas, and Hawaii. Expanding the validation test ground is especially beneficial to prospective operational and non-operational users of this frontal product. Indeed, other regions feature certain types of fronts that are not well represented off the U.S. Northeast. A few examples are: (a) river plumes of the Mississippi River (Gulf of Mexico), Columbia River (Washington-Oregon Shelf), and Yukon River (Bering Sea); (b) upwelling fronts off California; (c) leeway fronts in the Hawaii Islands wake.

(3) The quality of gradient *direction* output product could be improved by developing advanced median filters customized for gradient direction. Three possible improvements are suggested below:

3.1. **Increasing window size.** Computer experiments are needed with different sizes of the median filter window. Currently, the anisotropic median filter used in the SNRA is quite conservative: It is just 3 pixels wide (in the along-stripe direction) and 5 pixels tall (in the cross-stripe direction). We have chosen the

conservative approach (small window size) because one of our main goals was to avoid excessive smoothing of MODIS images, which is almost unavoidable when large windows are used. Yet, larger windows might be much more effective in suppressing (reducing) stripes in the gradient direction output product. Particularly, the window height increase up to 7 or even 9 might be quite effective. Generally speaking, the height of median filter window could be safely increased up to DBS (Distance Between Stripes or simply stripe spacing). This approach would work just fine provided the DBS remains constant across the image. In such cases, the algorithm could be fully automated by utilizing autocorrelation function to determine DBS, and then using a median filter with a height carefully chosen (automatically selected) to approximate DBS from below: height < DBS – SW, where SW is stripe width. Possible complications arise from two factors: (1) DBS sometimes vary across the same image; (2) SW could vary, albeit slightly, along the same stripe, and it could also vary across the same image. Possible solutions could include the development of a fully context-sensitive median filter whose parameters adapt to the changing parameters of stripes in the image.

3.2. **Customizing adaptive median filter for gradient direction.** Indeed, the nature of stripes in gradient direction fields is quite different from that of gradient magnitude. Namely, gradient direction changes 180 degrees (makes a U-turn) while crossing orthogonally over a stripe. This change is described by a step function. This model is different from that of gradient magnitude changes in the vicinity of stripes, which is more complicated and variable. Therefore, the development of an adaptive median filter for gradient direction is fully warranted. This filter will take advantage of the relative simplicity of striping pattern in gradient direction fields.

3.3. **Applying circular median filter to gradient direction.** Strictly speaking, the same median filter that works well with gradient magnitude should not be applied to gradient direction. The special nature of directional (circular or angular) data and the need for a special statistical theory of directional data have been recognized a while ago (Mardia, 1972; Fisher, 1996; Mardia and Jupp, 1999). The main cardinal difference between direction and magnitude is that direction is an inherently periodical physical quantity, whereas magnitude is not. Therefore the Cartesian ordering that works well in median filters applied to magnitude should not be used in filters intended for direction. Special circular filters have been developed for angular data (e.g., Nikolaidis and Pitas, 1998). Such filters can be applied to gradient direction in satellite oceanography. This has never been done before; therefore numerical experiments are required to choose the best filter or to develop a customized circular filter for the frontal product.

(4) Improvements in *quality assessment* can be achieved by including advanced metrics for monitoring the SNRA performance. One of such metrics is a measure of *relative improvement* of the SNRA output quality, RELIMP. The RELIMP differs from the aforementioned parameter NPIX (total number of pixels modified by SNRA) in that the RELIMP is basically NPIX normalized by the total number of valid pixels (pixels that contain valid data and are not cloud-masked or land-masked). Two other advanced parameters would calculate RELIMP and DIST2 (integrated pixel-based squared distance between the input and output images) for *stripe pixels* only. This step should await pattern recognition of stripes, which is a formidable task given the somewhat diffuse nature of stripes in MODIS images.

4. REFERENCES

Al-Amri, S.S., Kalyankar, N.V., Khamitkar, S.D. (2010). A comparative study of removal noise from remote sensing image. International Journal of Computer Science 7 (1), 32-36.

Belkin, I.M. (1986). Morpho-statistical objective classification of vertical profiles of hydrophysical parameters. Transactions of the Academy of Sciences of the USSR 286 (3), 707–711.

Belkin, I.M. (1991). *Morpho-Statistical Analysis of Ocean Stratification*. Gidrometeoizdat, St. Petersburg, 134 pp.

Belkin, I.M. (2002). Front. In: *Interdisciplinary Encyclopedia of Marine Sciences*, edited by James W. Nybakken, William W. Broenkow, and Tracy L. Vallier, Vol. 1, pp. 433-436, Grolier Academic Reference, Danbury, Conn.

Belkin, I.M., Cornillon, P.C. (2003). SST fronts of the Pacific coastal and marginal seas. Pacific Oceanography 1 (2), 90–113.

Belkin, I.M., Cornillon, P.C. (2004). Surface thermal fronts of the Okhotsk Sea. Pacific Oceanography 2 (1–2), 6–19.

Belkin, I.M., Cornillon, P.C. (2005). Bering Sea thermal fronts from Pathfinder data: seasonal and interannual variability. Pacific Oceanography 3 (1), 6–20.

Belkin, I.M., O'Reilly, J.E. (2009). An algorithm for oceanic front detection in chlorophyll and SST satellite imagery. Journal of Marine Systems 78(3), 319-326.

Belkin, I.M., Shan, Z., Cornillon, P. (1998). Global survey of oceanic fronts from Pathfinder SST and in-situ data. AGU 1998 Fall Meeting Abstracts. Eos 79 (45, Suppl.), F475.

Belkin, I.M., Cornillon, P., Shan, Z. (2001). Global survey of ocean fronts from Pathfinder SST data. Abstracts of the Oceanography Society Meeting, April 2–5, 2001, Miami Beach, FL. Oceanography 14 (1), 10.

Belkin, I.M., Cornillon, P.C., Ullman, D. (2003). Ocean fronts around Alaska from satellite SST data. Proceedings of the American Meteorological Society 7th Conference on the Polar Meteorology and Oceanography, Hyannis, MA, Paper 12.7. 15 pp.

Belkin, I.M., Cornillon, P.C., Sherman, K. (2009). Fronts in Large Marine Ecosystems. Progress in Oceanography 81 (1-4), 223–236.

Belkin, I.M., Hyde, K.J.W., O'Reilly, J.E. (2012). Satellite climatologies of chlorophyll and SST fronts off the U.S. East Coast (in preparation).

Bontempi, P.S., Yoder, J.A. (2004). Spatial variability in SeaWiFS imagery of the South Atlantic bight as evidenced by gradients (fronts) in chlorophyll a and water-leaving radiance. Deep-Sea Research II 51 (10–11), 1019–1032.

Bouali, M., Ladjal, S. (2011). Toward optimal destriping of MODIS data using a unidirectional variational model. IEEE Transactions on Geoscience and Remote Sensing 49 (8), 2924-2935.

Bovik, A.C. (1987) Streaking in median filtered images. IEEE Transactions on Acoustics, Speech, and Signal Processing 35 (4), 493-503.

Breaker, L.C., Mavor, T.P., Broenkow, W.W. (2005). Mapping and monitoring large-scale ocean fronts off the California Coast using imagery from GOES-10 geostationary satellite. Publication T-056, California Sea Grant College Program, University of California, San Diego. 25 pp., http://repositories.cdlib.org/csgc/rcr/Coastal05_02.

Campbell, J.W. (1995). The lognormal distribution as a model for bio-optical variability in the sea. Journal of Geophysical Research 100 (C7), 13237–13254.

Canny, J.F. (1986). A computational approach to edge detection. IEEE Transactions on Pattern Analysis and Machine Intelligence 8 (6), 679–698.

Castelao, R.M., Mavor, T.P., Barth, J.A., Breaker, L.C. (2006). Sea surface temperature fronts in the California Current System from geostationary satellite observations. Journal of Geophysical Research 111, C09026.

Cayula, J.-F., Cornillon, P. (1992). Edge detection algorithm for SST images. Journal of Atmospheric and Oceanic Technology 9 (1), 67–80.

Cayula, J.-F., Cornillon, P. (1995). Multi-image edge detection for SST images. Journal of Atmospheric and Oceanic Technology 12 (4), 821–829.

Cayula, J.-F., Cornillon, P. (1996). Cloud detection from a sequence of SST images. Remote Sensing of Environment 55 (1), 80–88.

Cayula, J.-F., Cornillon, P., Holyer, R., Peckinpaugh, S. (1991). Comparative study of two recent edge-detection algorithms designed to process sea-surface temperature fields. IEEE Transactions on Geoscience and Remote Sensing 29 (1), 175–177.

Celebi, M.E., Kingravi, H.A., Aslandogan, Y.A. (2007). Nonlinear vector filtering for impulsive noise removal from color images. Journal of Electronic Imaging 16 (3), 033008.

Chan, C.O. (1999). Spatial patterns in ocean color and temperature maps: fronts, fractals and ecological considerations. Ph.D. Thesis, Graduate School of Oceanography, University of Rhode Island, Narragansett, RI, 173 pp.

Curran, P.J., Dungan, J.L. (1989). Estimation of signal-to-noise: A new procedure applied to AVIRIS data. IEEE Transactions on Geoscience and Remote Sensing 21 (5),

Di Bisceglie, M., Episcopo, R., Galdi, C., Ullo, S.L. (2009). Destriping MODIS data using overlapping field-of-view method. IEEE Transactions on Geoscience and Remote Sensing 47 (2), 637-651.

Fisher, N.I. (1996). *Statistical Analysis of Circular Data*. Cambridge University Press, 296 pp.

Gallagher, N.C., Wise, G.L. (1981). A theoretical analysis of the properties of median filters. IEEE Transactions on Acoustics, Speech and Signal Processing 29 (6), 1136–1141.

Gladkova, I., Grossberg, M.D., Shahriar, F., Bonev, G., Romanov, P. (2012). Quantitative restoration for MODIS Band 6 on Aqua. IEEE Transactions on Geoscience and Remote Sensing 50 (6), 2409-2416.

Gregg, W.W., Conkright, M.E. (2001). Global seasonal climatologies of ocean chlorophyll: blending in situ and satellite data for the Coastal Zone Color Scanner era. Journal of Geophysical Research 106 (2), 2499–2515.

Gregg, W.W., Casey, N.W. (2004). Global and regional evaluation of the SeaWiFS chlorophyll data set. Remote Sensing of Environment 93 (4), 463–479.

Haralick, R.M., Sternberg, S.R., Zhuang, X.H. (1987). Image analysis using mathematical morphology. IEEE Transactions on Pattern Analysis and Machine Intelligence 9 (4), 532-550.

Hickox, R., Belkin, I.M., Cornillon, P.C., Shan, Z. (2000). Climatology and seasonal variability of ocean fronts in the East China, Yellow and Bohai Seas from satellite SST data. Geophysical Research Letters 27 (18), 2945–2948.

Hyde K., O'Reilly, J., Belkin, I. (2008). Satellite climatology of chlorophyll and SST fronts in the Northeast US Large Marine Ecosystem. AGU 2008 Ocean Sciences Meeting, Orlando (FL). 059-1293.

Holyer, R.J., Peckinpaugh, S.H. (1989). Edge detection applied to satellite imagery of the oceans. IEEE Transactions on Geoscience and Remote Sensing 27 (1), 46–56.

Juhola, M., Katajainen, J., Raita, T. (1991). Comparison of algorithms for standard median filtering. IEEE Transactions on Signal Processing 39 (1), 204-208.

Kahru, M., Hakansson, B., Rud, O. (1995). Distributions of the sea-surface temperature fronts in the Baltic Sea as derived from satellite imagery. Continental Shelf Research 15 (6), 663–679.

Kazmin, A.S., Rienecker, M.M. (1996). Variability and frontogenesis in the large-scale oceanic frontal zones. Journal of Geophysical Research 101 (C1), 907–921.

Kober, V., Mozerov, M., Álvarez-Borrego, J. (2003). Spatially adaptive algorithm for impulse noise removal from color images. In: Progress in Pattern Recognition, Speech and Image Analysis, pp. 113-120, Springer.

Konnik, M. (2009). Small survey of objective image quality metrics. Available online: http://www.mvkonnik.info/2009/03/small-survey-of-objective-image-quality.html .

Kostianoy, A.G., Ginzburg, A.I., Frankignoul, M., Delille, B. (2004). Fronts in the southern Indian Ocean as inferred from satellite sea surface temperature data. Journal of Marine Systems 45 (1–2), 55–73.

Kumar, V.R.V., Manikandan, S., Ebenezer, D., Vanathi, P.T., Kanagasabapathy, P. (2007). High density impulse noise removal in color images using median controlled adaptive recursive weighted median filter. International Journal of Computer Science 34 (1), 2.

Legeckis, R. (1978). A survey of worldwide sea surface temperature fronts detected by environmental satellites. Journal of Geophysical Research 83 (C9), 4501–4522.

Legeckis, R., Christopher, W.B., Chang, P.S. (2002). Geostationary satellites reveal motions of ocean surface fronts. Journal of Marine Systems 37 (1–3), 3–15.

Liu, C., Freeman, W.T., Szeliski, R., Kang, S.B. (2006). Noise estimation from a single image. Proceedings of the 2006 IEEE Computer Society Conference on Computer Vision and Pattern Recognition (CVPR'06).

Marra, J., Houghton, R.W., Garside, C. (1990). Phytoplankton growth at the shelf-break front in the Middle Atlantic Bight. Journal of Marine Research 48 (4), 851–868.

Mao, M., Gan, Z.J. (1993). Statistical analysis for the convergence rate of signals to median filter roots. IEEE Transactions on Signal Processing 41 (7), 2499-2502.

Mardia, K.V. (1972). *Statistics of Directional Data*. Academic Press, New York, 357 pp.

Mardia, K.V., Jupp, P.E. (1999) *Directional Statistics.* Wiley, Chichester etc., 350 pp.

Mavor, P.T., Bisagni, J.J. (2001). Seasonal variability of sea-surface temperature fronts on Georges Bank. Deep-Sea Research II 48 (1–3), 215–243.

Mélange, T., Nachtegael, M., Schulte, S., Kerre, E.E. (2011). A fuzzy filter for the removal of random impulse noise in image sequences. Image and Vision Computing 29 (6), 407-419.

Miller, P.I. (2004). Multi-spectral front maps for automatic detection of ocean colour features from SeaWiFS. International Journal of Remote Sensing 25 (7–8), 1437–1442.

Miller, P.I. (2009). Composite front maps for improved visibility of dynamic sea-surface features on cloudy SeaWiFS and AVHRR data. Journal of Marine Systems 78 (3), 327–336.

Moore, J.K., Abbott, M.R., Richman, J.G. (1997). Variability in the location of the Antarctic Polar Front (90°–20°W) from satellite sea surface temperature data. Journal of Geophysical Research 102 (C13), 27,825–27,834.

Moore, J.K., Abbott, M.R., Richman, J.G. (1999). Location and dynamics of the Antarctic Polar Front from satellite sea surface temperature data. Journal of Geophysical Research 104 (C2), 3059–3074.

Nichol, J.E., Vohora, V. (2004). Noise over water surfaces in Landsat TM images. International Journal of Remote Sensing 25 (11), 2087-2094.

Nieto, K., Demarcq, H. (2006). Multi-image edge detection on SST and chlorophyll satellite images in northern Chile. Workshop on Indices of Mesoscale Structures, 22–24 February 2006, IFREMER, Nantes, France. www.ices.dk/reports/occ/2006/wkims06.pdf .

Nikolaidis, N., Pitas, I. (1998). Nonlinear processing and analysis of angular signals. IEEE Transactions on Signal Processing 46 (12), 3181-3194.

Olsen, S.I. (1993). Estimation of noise in images: An evaluation. CVGIP: Graphical Models and Image Processing 55 (4), 319-323.

Qiu, G.P. (1996). An improved recursive median filtering scheme for image processing. IEEE Transactions on Image Processing 5(4), 646-648.

Rakwatin, P. Takeuchi, W., Yasuoka, Y. (2007). Stripe noise reduction in MODIS data by combining histogram matching with facet filter. IEEE Transactions on Geoscience and Remote Sensing 45 (6), 1844-1856.

Rakwatin, P. Takeuchi, W., Yasuoka, Y. (2009). Restoration of Aqua MODIS Band 6 using histogram matching and local least squares fitting. IEEE Transactions on Geoscience and Remote Sensing 47 (2), 613-627.

Russell, R., Sinha, P. (2001). Perceptually-based comparison of image similarity metrics. MIT, Artificial Intelligence Laboratory, AI Memo 2001-014/CBCL Memo 201, 13 pp.

Ryan, J.P., Yoder, J.A., Cornillon, P.C. (1999a). Enhanced chlorophyll at the shelfbreak of the Mid-Atlantic Bight and Georges Bank during the spring transition. Limnology and Oceanography 44 (1), 1–11.

Ryan, J.P., Yoder, J.A., Cornillon, P.C., Barth, J.A. (1999b). Chlorophyll enhancement and mixing associated with meanders of the shelf break front in the Mid-Atlantic Bight. Journal of Geophysical Research 104 (C10), 23479–23493.

Sahasrabudhe, N., West, J.E., Machiraju, R., Janus, M. (1999). Structured spatial domain image and data comparison metrics. VIS'99 Proceedings of the Conference on Visualization '99: celebrating ten years, pp. 97-104. IEEE Computer Society Press, Los Alamitos, CA.

Shen, H.F., Zhang, L.P. (2009). A MAP-based algorithm for destriping and inpainting of remotely sensed images. IEEE Transactions on Geoscience and Remote Sensing Volume 47 (5), 1490-1500.

Shen, H.F., Zeng, C., Zhang, L.P. (2011). Recovering reflectance of Aqua MODIS Band 6 based on within-class local fitting. IEEE Journal of Selected Topics in Applied Earth Observations and Remote Sensing 4 (1), 185-192.

Shimada, T., Sakaida, F., Kawamura, H., Okumura, T. (2005). Application of an edge detection method to satellite images for distinguishing sea surface temperature fronts near the Japanese coast. Remote Sensing of Environment 98 (1), 21–34.

Stegmann, P.M., Ullman, D.S. (2004). Variability in chlorophyll and sea surface temperature fronts in the Long Island Sound outflow region from satellite observations. Journal of Geophysical Research 109, C07S03.

Stork, M. (2003). Median filters theory and applications. In: ELECO 2003. Istanbul, UMUT Matbaacilik, 233-237. ISBN 975-395-667-3. www.emo.org.tr/ekler/2130c418d4f02c7_ek.pdf

Tai, S.C, Yang, S.M. (2008). A fast method for image noise estimation using Laplacian operator and adaptive edge detection. Proceedings of the 3rd International Symposium on Communications, Control and Signal Processing (ISCCSP 2008), pp. 1077-1081.

Takahashi, W., Kawamura, H. (2005). Detection method of the Kuroshio front using the satellite-derived chlorophyll-a images. Remote Sensing of Environment 97 (1), 83–91.

Tsai, F., Chen, W.W. (2008). Striping noise detection and correction of remote sensing images. IEEE Transactions on Geoscience and Remote Sensing 46 (12), 4122-4131.

Ullman, D.S., Cornillon, P.C. (1999). Surface temperature fronts off the East Coast of North America from AVHRR imagery. Journal of Geophysical Research 104 (C10), 23459–23478.

Ullman, D.S., Cornillon, P.C. (2000). Evaluation of front detection methods for satellite-derived SST data using in situ observations. Journal of Atmospheric and Oceanic Technology 17 (12), 1667–1675.

Ullman, D.S., Cornillon, P.C. (2001). Continental shelf surface thermal fronts in winter off the northeast US coast. Continental Shelf Research 21 (11–12), 1139–1156.

Vazquez,D.P., Atae-Allah, C., Luque-Escamilla, P.L. (1999). Entropic approach to edge detection for SST images. Journal of Atmospheric and Oceanic Technology 16 (7), 970–979.

Wang, Z., Bovik, A.C. (2002). A universal image quality index. IEEE Signal Processing Letters 9 (3), 81-84.

Williamson, G.A., Clarkson, P.M., Sethares, W.A. (1993). Performance characteristics of the median LMS adaptive filter. IEEE Transactions on Signal Processing 41 (2), 667-680.

Wilson, D.L., Baddeley, A.J., Owens, R.A. (1997). A new metric for grey-scale image comparison. International Journal of Computer Vision 24 (1), 5-17.

Wu, J., Tang, C. (2011). An efficient decision-based and edge-preserving method for salt-and-pepper noise removal. Pattern Recognition Letters 32 (15), 1974-1981.

Yang, J.F., Zhang, Y., Yin, W.T. (2009). An efficient TVL1 algorithm for deblurring multichannel images corrupted by impulsive noise. SIAM Journal of Scientific Computing 31 (4), 2842–2865.

Yang, N.H.C., Lai, A.H.S. (1996). Performance evaluation of a feature-preserving filtering algorithm for removing additive random noise in digital images. Optical Engineering 35 (7), 1871-1885.

Zhou, H.L., Chen, M., Webster, M.F. (2002). Comparative evaluation of visualization and experimental results using image comparison metrics. VIS '02 Proceedings of the Conference on Visualization '02, pp. 315 – 322. IEEE Computer Society, Washington, DC.

========== end of document ==========